

27 **Abstract**

28

29 *Ruminococcus gnavus* is a human gut symbiont which ability to degrade mucins is mediated
30 by an intramolecular *trans*-sialidase (*RgNanH*). *RgNanH* comprises a GH33 catalytic domain
31 and a sialic acid binding carbohydrate binding module (CBM40). Here we used glycan
32 arrays, STD NMR, X-ray crystallography, mutagenesis, and binding assays to determine the
33 structure and function of *RgNanH*_CBM40 (*RgCBM40*). *RgCBM40* displays the canonical
34 CBM40 β -sandwich fold and broad specificity towards sialoglycans with millimolar binding
35 affinity towards α 2,3- or α 2,6-sialyllactose. *RgCBM40* binds to mucus produced by goblet
36 cells and to purified mucins, providing direct evidence for a CBM40 as a novel bacterial
37 mucus adhesin. Bioinformatics data show that *RgCBM40* canonical type domains are
38 widespread among Firmicutes. Furthermore, binding of *R. gnavus* ATCC 29149 to intestinal
39 mucus is sialic acid mediated. Together, this study reveals novel features of CBMs which
40 may contribute to the biogeography of symbiotic bacteria in the gut.

41

42

43

44 Introduction

45 The human gut microbiota encompasses a complex community of bacterial species which
46 play a critical role in human health, through their contribution to e.g. polysaccharide
47 digestion, immune system development, pathogen defence¹. Microbiota composition varies
48 longitudinally along the gastrointestinal (GI) tract but also transversally from the lumen to the
49 mucosa^{1,2}. Most gut bacteria reside in the colon, reaching 10^{11} to 10^{12} cells per gram, where
50 they compete for dietary and host glycans^{3,4}. A dysbiosis of the gut microbiota is associated
51 with intestinal diseases, including cancers, infections, and inflammatory bowel diseases⁵⁻⁸,
52 underscoring the importance of understanding these host-microbe interactions in order to
53 devise novel treatment strategies.

54 Several factors influence the biogeography of symbiotic bacteria within the gut, including the
55 gradient and availability of glycans within discrete physical niches^{2,3}. The mucus layer
56 covering the GI tract is at the interface between the gut microbiota and the host⁵. In the
57 colon, the mucus layer is divided into a loose outer layer providing a habitat to commensal
58 bacteria and an inner layer adhering to the epithelium and providing protection from bacterial
59 invasion⁵. The outer mucus layer hosts a distinct intestinal microbial niche⁹. The intestinal
60 mucus layers are built around large highly glycosylated gel-forming mucin MUC2 (Muc2 in
61 mouse) secreted by goblet cells¹⁰. The glycan structures present in mucins are diverse and
62 complex and consist of four core mucin-type O-glycans containing *N*-acetylgalactosamine
63 (GalNAc), galactose (Gal) and *N*-acetylglucosamine (GlcNAc). Mucin O-glycosylation starts
64 with the attachment of GalNAc residues to the hydroxyl group of Ser and Thr of the protein
65 backbone to form the Tn antigen (GalNAc α 1-Ser/Thr). This glycan is then elongated into
66 core 1 (Gal β 1-3GalNAc α 1-Ser/Thr, also known as Thomsen Friedenreich-TF- or T-antigen),
67 core 2 (Gal β 1-3(GlcNAc β 1-6)GalNAc α 1-Ser/Thr), core 3 (GlcNAc β 1-3GalNAc α 1-Ser/Thr) or
68 core 4 (GlcNAc β 1-3(GlcNAc β 1-6)GalNAc α 1-Ser/Thr)¹¹. Core 3-derived O-glycans are
69 important components of human colonic mucin-type O-glycans¹². These core structures are
70 further elongated by the addition of other carbohydrates (e.g. *N*-acetylglucosamine, LacNAc)
71 and are most commonly terminated by fucose and sialic acid sugar residues *via* α 1-2/3/4
72 and α 2-3/6 linkages, respectively. These oligosaccharide chains provide binding sites and
73 nutrients to the bacteria which have adapted to the mucosal environment^{13,14}. Reflecting the
74 structural diversity of mucin glycans and their prime location, commensal and pathogenic
75 microbes have evolved a range of adhesins allowing their interaction with mucus^{13,15}.
76 Variation in mucosal carbohydrate availability leads to variations in the composition of the
77 resident microbiota^{3,16,17} and may also impact on bacterial tropism along and across the GI
78 tract¹⁸.

79 Sialic acids such as *N*-acetylneuraminic acid (Neu5Ac) and fucose residues in terminating
80 positions on mucin glycan chains are prominent targets for commensal and pathogenic
81 bacteria^{19,20}. The ratio of sialic acid to fucose increases along the GI tract, from the ileum to
82 the rectum in humans²¹ and an inverse gradient occurs in mice²². Furthermore blood group
83 Sd^a/Cad related epitopes, GalNAcβ1-4(NeuAcα2-3)Gal, increase along the length of the
84 human colon¹². Over 100 complex oligosaccharides can be identified in mucins from human
85 colonic biopsies, with most mono-, di- or trisialylated²³. Release of sialic acid by microbial
86 sialidases allows bacteria to access free sialic acid for catabolism, decrypt host ligands for
87 adherence, participate in biofilm formation, modulate immune function by metabolic
88 incorporation, and expose the underlying glycans for further degradation^{10,14,19,20}. Sialidases
89 are often associated with additional domains including carbohydrate binding modules
90 (CBMs) such as sialic acid specific CBM40^{14,24} and broadly specific CBM32²⁵. CBMs can
91 enhance catalytic activity by concentrating the enzymes onto carbohydrate substrates²⁶ or
92 mediate adherence to host cells²⁷.

93 *Ruminococcus gnavus* is a prominent member of the gut microbiota of the healthy human
94 gut²⁸. *R. gnavus* utilisation of mucin is associated with the expression of an intramolecular
95 *trans*-sialidase (IT-sialidase)^{29,30}, which is proposed to play a key role in the adaptation of gut
96 bacteria to the mucosal environment by providing 2,7-anhydro-sialic acid as a preferential
97 source of nutrients³¹. The IT-sialidase from *R. gnavus* ATCC 29149 (*RgNanH*) comprises a
98 catalytic glycoside hydrolase domain, *RgGH33* and a carbohydrate binding module,
99 *RgCBM40*.

100 Here, to gain insights into the role and specificity of sialic acid recognition by *R. gnavus*, we
101 employed glycan microarray, X-ray crystallography, saturation transfer difference nuclear
102 magnetic resonance spectroscopy (STD NMR), isothermal titration calorimetry (ITC),
103 mutational analyses, and cell/tissue binding assays to identify *RgCBM40* oligosaccharide
104 binding partners. Prominent ligands were oligosaccharides with terminal sialic acid, including
105 those which are not substrates for *RgNanH* activity. We propose a novel role for CBM40 in
106 targeting gut bacteria towards sialic acid-rich regions of the GI tract.

107
108
109
110
111
112

113 **Results**

114

115 ***Rg*CBM40 belongs to the CBM40 subfamily**

116 *Rg*CBM40 crystallised as a dimer, adopting the canonical CBM40 β -sandwich fold with six
117 antiparallel strands on the convex face and five on the concave face (**Fig. 1a**, for data
118 collection and refinement statistics, see **Table 1**). Electron density was observed for all
119 *Rg*CBM40 residues present in the construct (50–237). The sialic acid binding site is on the
120 concave face at the dimer interface (**Fig. 1b**), however size exclusion chromatography with
121 multi angle light scattering (SEC-MALS) indicated that the full-length protein, *Rg*NanH, is
122 monomeric in solution (**Fig. 1c**). The macromolecular architecture of *Rg*CBM40 is conserved
123 among members of the CBM40 family (**Supplementary Fig. 1**), with the exception of *Vibrio*
124 *cholerae* CBM40_NanH (*Vc*CBM40_NanH) which is proposed to be part of a separate
125 CBM40 subfamily (**Supplementary Fig. 1h**)^{25,32}. Greatest structural homology was observed
126 to *Md*CBM40 NanL (RMSD: 0.3 Å) from the *Macrobodella decora* IT-sialidase
127 (**Supplementary Fig. 1e**)³³.

128 Protein ligand complexes were achieved for both 3'SL and 6'SL (**Fig. 1d and e**). No
129 significant conformational changes were observed in the binding site upon ligand binding.
130 Definitive electron density for the Neu5Ac and galactose residues was observed in the 3'SL
131 and 6'SL complexes. In the 6'SL complex, electron density was also observed for the
132 glucose residues (**Fig. 1e**), with the lactose positioned almost perpendicular to the sialic acid
133 (**Fig. 1e**). Contrastingly, for the 3'SL complex, only partial electron density was observed for
134 the glucose residue in a single monomer (**Fig. 1d**), and the glucose positioning indicates that
135 the lactose points up and away from the binding site, without further interactions with the
136 protein. In the 3'SL complex, the lactose positioning would permit further extensions to the
137 carbohydrate chain as would be present in more complex or anchored glycans, whereas
138 these may be blocked in the 6'SL complex. This would provide a degree of specificity
139 towards sialic acid linkage.

140 Neu5Ac binds in a chair conformation (**Fig. 1f and g**), mimicking the solution conformation
141 and minimizing the energetic penalty paid upon binding²⁶. Notably, the carboxylic acid group
142 of Neu5Ac forms electrostatic interactions with an arginine dyad, Arg204 and Arg128,
143 mimicking the coordination observed in sialidase active sites. The C4 hydroxyl group
144 hydrogen bonds to Lys135 and Glu126, the N-acetyl group sits in a hydrophobic pocket
145 formed by Tyr116 and Ile95. The N-acetyl group nitrogen interacts with both Glu126 and
146 Tyr210. Glu126, Arg128, and Arg204 make extensive interactions with the bound ligand and
147 are conserved in all structurally characterized CBM40 sialic acid binding sites, discounting
148 *Vc*CBM40_NanH³⁴ (**Supplementary Fig. 2**). The environment of the glycerol side-chain of

149 sialic acid is generally conserved across the canonical CBM40 subfamily with the rear face
150 (C7-H and C9-H groups) residing on a hydrophobic surface formed by Ile95 and Tyr210 in
151 *Rg*CBM40 (**Supplementary Fig. 3a**). Although *Vc*CBM40_NanH shares the CBM40 β -
152 sandwich fold (**Supplementary Fig. 1**), the location, orientation, and constitution of its sialic
153 acid binding site is not conserved (**Supplementary Fig. 2**).

154

155 **Structure-based sequence alignment**

156 CBM40s associated with sialidases fall into two subfamilies, the canonical subfamily
157 exemplified by *Cp*CBM40_NanJ²⁵ (which also regroups *Rg*CBM40, *Cp*CBM40_NanI³²,
158 *Sp*CBM40_NanA³⁵, *Sp*CBM40_NanB³⁶, *Sp*CBM40_NanC³⁷ and *Md*CBM40_NanL³³), and the
159 *Vibrio* subfamily exemplified by *Vc*CBM40_NanH³⁴. Considerable sequence divergence
160 between the *Vibrio* and canonical CBM40 types renders satisfactory alignments difficult to
161 produce with standard tools, as also previously reported³². Here, by detailed manual
162 inspection, paying particular attention to the limits of secondary structure elements and
163 intervening loops, we produced an alignment of both types of CBM40 sequences showing
164 well-conserved positions along its length, notwithstanding the *Vibrio* insertion (40 residues)
165 near the N-terminus. The pairwise identities between the canonical representatives range
166 from 21–67%, while the maximum canonical versus *Vibrio* identity is 17%, reflecting that
167 CBM40s fall into two distinct groups. This highlighted conserved residues within the
168 canonical subfamily that may be involved in binding affinity and specificity (**Fig. 2**). These
169 include (*Rg*CBM40 numbering): an arginine dyad (Arg204 and Arg128) that interacts with
170 the sialic acid carboxylic acid group, a glutamic acid (Glu126), which hydrogen bonds to the
171 C4 hydroxyl; and a hydrophobic surface, which accommodates the N-acetyl moiety and the
172 hydrophobic face of the glycerol group. Tyr116, Ile95, Tyr210 contribute to the surface of an
173 aromatic:aliphatic:aromatic twisted platform which presents the glycerol hydroxyl groups to
174 solvent²⁶.

175 **Bioinformatics analyses**

176 To gain further insights into the phylotypic distribution of the CBM40 domains within bacterial
177 genomes, we performed a database search using pHMMs derived from our alignment as
178 queries (canonical and *Vibrio*-type together, referred to as 'combined'; canonical only; *Vibrio*-
179 type only) as well as Pfam models, "Sialidase(NTD)", "Laminin_G_3", and "Sial-lect-inser"
180 (see **Methods** and **Supplementary Methods**). Our combined model successfully identified
181 99.9% of the CBM40 domains matched by the individual type CBM40 models (over 16,000
182 domain hits in the whole database of around 67,000 genomes). Further analysis of the data
183 (see **Supplementary Methods**) led to the identification of 51 nonredundant sequences
184 (**Supplementary Fig. 4**). Of these, the canonical CBM40 domains occurred in Firmicutes

185 with 40 sequences, representing 18 genera or pseudogenera, divided between classes
186 Bacilli and Clostridia, as well as Erysipelotrichi and an unclassified member of the
187 Firmicutes; and two sequences in Actinobacteria. The Vibrio type occurred only in
188 Gammaproteobacteria, represented by 8 sequences in five genera. The separation between
189 the Vibrio-type sequences and canonical CBM40 sequences across bacterial genomes was
190 also apparent from a tree representation constructed using a simple distance-based model
191 and neighbour-joining (**Fig. 3**). This dichotomy was fully supported by bootstrap analysis of
192 1,000 replicates. There was no evidence for any intermediate or other CBM40 types. Only
193 one sequence from *Actinobacillus muris* containing a canonical CBM40 (confirmed by
194 pHMMs and conserved binding residues) was shown to be part of a Gammaproteobacteria
195 clade (all other members Vibrio type) as supported by 79% of bootstraps. Further studies
196 may indicate whether this domain is the closest to an inferred common ancestor of the
197 canonical and Vibrio CBM40 types. The results for co-incidence of sialidase domains clearly
198 indicated an association with CBM40s in this set of nonredundant sequences: we detected a
199 sialidase domain in 92% of canonical-type CBM40 and in all Vibrio type CBM40
200 representatives.

201

202 ***Rg*CBM40 preferentially binds α 2,3 linked sialosides**

203 To further explore *Rg*NanH ligand specificity, *Rg*CBM40 and inactive mutant *Rg*GH33
204 D282A, were tested for binding to various sialoglycans, using a slide microarray^{38,39}. This
205 sialoglycan microarray presents over 60 synthetically recreated naturally-occurring
206 oligosaccharide structures with diverse sialic acid forms, glycosidic linkages, and underlying
207 glycans, representing a broad range of such targets^{38,39}. Both recombinant proteins
208 exclusively bound to glycans terminated with sialic acids (**Fig. 4**). They also showed distinct
209 specificities. *Rg*CBM40 bound to terminal Neu5Ac, Neu5Gc, Neu5,9Ac₂ and 2-keto-3-
210 deoxynonulosonic acid (Kdn) attached with α 2-3, α 2-6 and α 2-8 linkages (**Fig. 4**). In
211 contrast, *Rg*GH33 D282A interacted weakly with a narrow spectrum of sialoglycans, mainly
212 α 2-3-Neu5Ac-containing glycans, primarily Neu5Ac α 3LacNAc β (3'SLN),
213 Neu5Ac α 3Gal β 3GlcNAc β , Neu5Ac α 3Gal β 3GalNAc (STF), Neu5Ac α 3Lac β (GM3), and
214 Neu5Ac α 3Gal β 3GalNAc β 3Lac (**Fig. 4**). Noticeably, *Rg*GH33 D282A recognized some of the
215 α 2-3-linked sialoglycans but not any α 2-6- or α 2-8-linked ones, in line with its substrate
216 specificity³⁰. In marked contrast, every α 2-3-linked sialyl oligosaccharide present on the
217 array could be bound by *Rg*CBM40. *Rg*CBM40 showed a preference for terminal Neu5Ac
218 over Neu5Gc, and for α 2-3>> α 2-6> α 2-8 linkages. *Rg*CBM40 bound generally more strongly
219 to glycans containing LacNAc and Lac. *Rg*CBM40 could bind Neu5Ac linked Lac with α 2-3
220 and α 2-6 linkage, albeit to a lesser degree, whereas binding to Neu5Ac linked LacNAc was

221 α 2-3-specific. Due to the glycan orientation introduced by the α 2-6-sialic acid linkage the
222 6'SL glucose residue is close to the protein surface (**Fig. 1e**). Therefore, α 2-6-linked LacNAc
223 *N*-acetyl group may be blocked by protein residues, whereas the α 2-3 linked glycan would
224 be more solvent exposed. The highest binding was to Neu5,9Ac₂ α 3Gal β R1. Interestingly,
225 *RgCBM40* bound to Neu5Gc α 3Gal β 3GalNAc β R1 (Neu5Gc-TF) and
226 Neu5Gc9Ac α 3Gal β 3GalNAc β R1 (Neu5Gc9Ac-TF) although with 5–10 fold less intensity, but
227 it could not bind to the same ligands with the α R1 linkage. *RgCBM40* bound to α 2-3-
228 sialylated Lewis X (3'SLX, both Neu5Ac and Neu5Gc forms, although Neu5Ac was
229 preferred). Sulfation of the 6 position of GlcNAc in 3'SLX (both Neu5Ac and Neu5Gc)
230 improved binding of the protein (**Fig. 4**).

231 To validate some of the glycan array data, we used STD NMR spectroscopy^{40,41} against a
232 range of sialylated ligands. Since the highest STD intensities correlate with the closest
233 ligand-protein contacts in the bound state⁴², STD NMR experiments provide important
234 information on the binding epitope of the complexed ligand⁴³.

235 Here Neu5Ac, Neu5Gc, 2,7-anhydro-Neu5Ac, 3'SL, 6'SL, Neu5Ac α 3Gal (3'SGal),
236 Neu5Ac α 6Gal (6'SGal), 3'SLN, Neu5Ac α 6LacNAc (6'SLN), Neu5Gc α 3Lac (3'SLGc),
237 Neu5Gc α 6Lac (6'SLGc), Neu5Ac α 6Gal α OC3H6N3 (Neu5Ac-STn),
238 Neu5Gc α 6Gal α OC3H6N3 (Neu5Gc-STn), and STF α OC3H6N3 were tested as potential
239 ligands for *RgCBM40*. With the exception of the three monosaccharides, Neu5Ac, Neu5Gc,
240 and 2,7-anhydro-Neu5Ac, binding to *RgCBM40* was detected for all di- and tri-saccharides
241 tested. For the latter, the binding epitope mapping was obtained and analyzed as described
242 under Methods. **Fig. 5a** shows the STD NMR spectra of 3'SL and 6'SL, and **Fig. 5b** their
243 binding epitope mapping. The sialic acid ring was found to be the main recognition element
244 and the binding mode was not affected by the nature of the glycosidic linkage (α 2-3 or α 2-6)
245 of the sialoglycan (**Supplementary Fig. 5**). The same was true for the other Neu5Ac-ending
246 ligands tested (see binding epitope mapping in **Supplementary Fig. 6**). The overall binding
247 epitopes of 3'SL and 6'SL from the STD NMR in solution state are in good agreement with
248 the crystal structures (**Fig. 5**), where the sialic acid is in close contact to the protein surface
249 while the lactose moiety is solvent exposed as suggested from the very low STD intensities
250 observed for the galactose and glucose protons. Very strong STD intensity is observed at
251 the methyl group (**Fig. 5**). This is in excellent agreement with the *N*-acetyl group sitting in the
252 hydrophobic pocket facing many protein protons (H δ and H γ) from the side chains of Ile95,
253 Tyr116, and Tyr210 (**Fig. 1f and 1g**). High intensity on H7 compared to the much lower one
254 on the adjacent H8 agrees with H7 facing the hydrophobic side chains while H8 (**Fig. 5**), in
255 *trans*-conformation to it, is pointing towards the solvent. Within experimental error, no stark
256 differences were observed in the orientation of the sialic acid ring in the binding pocket of

257 *RgCBM40*. *RgCBM40* also showed binding to Neu5Gc-ending oligosaccharides, albeit with
258 a lower strength. **Fig. 5c** shows the binding epitope of 3'SLGc and 6'SLGc (STD spectra are
259 shown in **Supplementary Fig. 6**). Again, sialic acid was the main recognition element of
260 these sialoglycans, but the binding epitope mapping was slightly different, in comparison to
261 those of 3'SL and 6'SL. For the Neu5Gc-ending ligands, stronger STD intensities on H3s
262 and lower ones on H6 were observed, suggesting a small reorientation of the ring around
263 C3, which would expose C6, in order to fit the bulkier hydroxyl group on the acetamide
264 moiety.

265 The affinity of the interaction between *RgCBM40* and sialic acid ligands was further
266 assessed by ITC. Both 3'SL and 6'SL bound with similar low affinities, with dissociation
267 constants of 0.57 mM and 1.70 mM, respectively (**Fig. 6a and b, Supplementary Table 1**).
268 This confirms that *RgCBM40* is specific for the terminal residue irrespective of the glycosidic
269 linkage but with a slight preference (~ 3 fold) for the 2-3 linkage. Furthermore, it would
270 suggest that the additional binding interactions observed in the crystal structure of the
271 complex between *RgCBM40* and 6'SL do not significantly promote binding, also in
272 agreement with the STD NMR results, showing that sialic acid is the main binding epitope in
273 solution. We confirmed that *RgCBM40* binds to Neu5Gc-oligosaccharides, albeit with lower
274 affinity, in accordance with the glycan array and STD NMR results. *RgCBM40* has a K_d of
275 ~3 mM and >10 mM towards 3'SLGc and 6'SLGc, respectively (**Fig. 6c, Supplementary**
276 **Table 1**). Very weak (~20 mM) interaction was observed between *RgCBM40* and Neu5Ac
277 (**Fig. 6d**) or Neu5Gc monosaccharides (**Supplementary Table 1**). The STD NMR
278 experiments were carried out with 1 mM sugar, well below the K_d, which explains why no
279 interaction was observed using this approach. Thermodynamic analysis showed that the
280 reaction is enthalpy-driven (**Supplementary Table 2**).

281 To further assess the involvement of individual residues we introduced point mutations
282 specifically designed to abrogate CBM binding. Arg128, Arg204, Tyr116, Tyr 210, Glu126
283 and Ile95 were chosen for alanine substitutions. Analysis of the secondary structure by
284 circular dichroism (CD) suggests that the recombinant proteins were correctly folded
285 (**Supplementary Fig. 7**). Binding to Neu5Ac, 3'SL and 6'SL was abolished for the double
286 mutant R128A/R204A as well as all single mutants, with the exception of I95A as shown by
287 ITC (**Supplementary Fig. 8a and b, Supplementary Table 1**). I95A binds 3'SL and 6'SL
288 with a K_d of 1.82 and 1.37 mM, respectively, broadly similar to the binding of the wild type
289 enzyme (**Supplementary Table 1**). This suggests that Ile95 is not an essential component of
290 the hydrophobic pocket or the aromatic:aliphatic:aromatic twisted platform, and that the Tyr
291 residues may compensate for the mutation of Ile95 to Ala. The binding ability of I95A to 3'SL
292 and 6'SL was further confirmed by STD-NMR (**Supplementary Fig. 9**).

293 Taken together, the STD NMR and ITC data confirmed binding of both α 2-3 and α 2-6 linked
294 sugars and raise questions regarding differences in ligand specificity between the catalytic
295 and carbohydrate binding domains constituting *RgNanH*. We previously showed that
296 *RgNanH* is specific for α 2-3-linked substrates³⁰. To determine the influence of *RgCBM40* on
297 the sialidase activity, we compared the enzymatic activity of *RgNanH* and *RgGH33* on a
298 range of sialylated substrates. The reaction was monitored by HPAEC-PAD and showed no
299 difference in catalytic activity on short oligosaccharides 3'SL, 3'SLX (Neu5Ac form) or on
300 large polymeric MUC2 mucins (**Supplementary Fig. 10**), indicating that, in the conditions
301 tested, *RgCBM40* did not potentiate the enzyme activity on these substrates.
302

303 ***RgCBM40* is a novel bacterial mucus adhesin**

304 *R. gnavus* ATCC 29149 but not the E1 strain encodes the IT-sialidase required for mucin-
305 degradation^{29,30}. Immunogold labeling and western blotting confirmed the presence of
306 *RgNanH* on *R. gnavus* ATCC 29149 cell-surface but not E1 (**Supplementary Fig. 11a and**
307 **b**). Given the role of *RgNanH* in *R. gnavus* mucin glycan utilization, the binding of *RgCBM40*
308 was tested towards a range of mucins with different glycosylation profiles by ELISA. The
309 sialylation level of purified commercial pig gastric mucin (pPGM), mixed and Muc2/MUC2
310 mucins from mice and LS174T human cell line was analyzed by mass spectrometry (MS),
311 revealing that most of the mucins tested contained >8% sialylated structures; pPGM and
312 Muc2 from the colon of wild type C57BL/6 mice contained <2% sialylated structures whereas
313 the level of sialylation of LS174T MUC2 reaches 91% (**Supplementary Table 3**). Highest
314 binding was observed to LS174T MUC2 whereas binding was lowest to pPGM or Muc2 from
315 the colon of wild type mice, which contain low levels of sialylation (**Fig. 7a**). The interaction
316 was dependent on the concentration of *RgCBM40* (**Supplementary Fig. 12**). *RgCBM40*
317 generally bound more strongly to mucins extracted from *C3GnT*^{-/-} mice (mutants which lack
318 core 3 β 1-3-N-acetylglucosaminyltransferase, C3GnT)⁴⁴ than to mucins from wild type mice.
319 Irrespective of the mouse model, the binding of *RgCBM40* to Muc2 from the small intestine
320 was higher than from the colon (**Fig. 7a**). The adhesion level correlated well with the level of
321 sialylation between the different mucins tested ($r^2 = 0.88$; **Fig. 7b**). *RgCBM40* bound
322 significantly less strongly to MUC2 which has been treated with trifluoroacetic acid (TFA) to
323 remove sialic acid, or with any of the sialidases tested which included the broad-specificity
324 sialidase from *Clostridium perfringens* (*Cp*) and the α 2-3-specific sialidases from *Salmonella*
325 *typhimurium* (*St*), *Akkermansia muciniphila* (*Ak*) and *R. gnavus* (*Rg*), confirming the
326 specificity of *RgCBM40* for terminal sialic acid (**Fig. 7c**). Consistent with the low affinity of
327 CBM40 for Neu5Ac, this monosaccharide had no effect on adherence of *RgCBM40* to mucin
328 (**Fig. 7d**). However, addition of free 3'SL or 6'SL prior to binding significantly decreased

329 adherence of *RgCBM40* to MUC2 (**Fig. 7d**). These data indicate that *RgCBM40* recognizes
330 sialylated mammalian mucins.

331 Having shown that *RgCBM40* can bind to sialylated oligosaccharides and mucins, we tested
332 its ability to bind to mucus from mouse intestinal tissue and human cell lines cells by
333 immunofluorescence (**Fig. 8**). Methacarn fixation allowed preservation of mucus in both
334 tissue sections and cell lines. Strong binding was demonstrated to mucus produced by
335 LS174T which correlated with staining patterns of SNA (a sialic acid specific lectin) and
336 MUC2 (**Fig. 8a**). No staining was observed in negative controls (*RgCBM40* free). *RgCBM40*,
337 Muc2 and lectin staining was also observed in crypts as well as on the epithelial surface of
338 mouse colonic tissue (**Fig. 8b**). In addition, sialidase treatment of mouse colonic sections
339 markedly reduced the binding of *RgCBM40* as well as the SNA lectin control (**Fig. 8c**). SNA
340 can outcompete *RgCBM40* binding to the mucus layer in mouse colonic tissue sections,
341 further indicating that the binding of *RgCBM40* to mucus is sialic acid mediated (**Fig. 8d**).
342 Similar inhibition was observed when using bacterial cells. *R. gnavus* ATCC 29149 was
343 shown to bind to areas that correlated with mucus staining. This binding was blocked with
344 the addition of SNA (**Fig. 8e**), confirming the importance of sialic acid recognition in *R.*
345 *gnavus* ATCC 29149 binding to mucus.

346

347 **Discussion**

348 Sialic acids are often found capping mammalian glycans and are thus common binding
349 targets of commensal or invading microbes. A wide variety of microorganisms utilize CBM-
350 containing sialidases to process these terminal sialic acid residues. At present CBMs in
351 family 40 are the only known examples to bind sialic acid and are exclusively associated
352 with sialidases (www.cazy.org). The CBM40 from *R. gnavus*, *RgCBM40*, adopts the
353 characteristic CBM40 β -sandwich fold, previously reported for CBM40s present in *C.*
354 *perfringens*^{25, 32}, *V. cholerae*³⁴, *M. decora*³³ as well as *S. pneumoniae*^{35,36,37}.

355 In their description of *C. perfringens* CpCBM40_NanJ, Boraston *et al.* pointed out that there
356 appears to be two subfamilies within the CBM40 family, one typified by CpCBM40_NanJ and
357 the other by *V. cholerae* VcCBM40_NanH²⁵. This was further supported by phylogenetic
358 analyses of all CBM40 structurally characterized so far³². It is clear that *Vibrio* sp. forms an
359 outlying clade in the family that has very low amino acid sequence identity (<15%) with the
360 main clade³². Here, we showed that the separation between the *Vibrio*-type sequences and
361 canonical CBM40 sequences is also observed across bacterial genomes. Both types adopt
362 a β -sandwich fold, however this is the most common core fold across CBM families²⁶.

363 *RgCBM40* crystal structures, of the canonical type, in complex with sialylated ligands

364 demonstrate shared core binding site residues. In brief, on one side of the sialic acid
365 residue, the carboxylic acid and C4 hydroxyl groups are coordinated by an arginine dyad
366 (Arg128 and Arg204) and a glutamic acid (Glu126) residue, respectively. The importance of
367 the arginine residues was further confirmed by mutational analyses, showing loss of binding
368 of *RgCBM40* R204A, *RgCBM40* R128A and the double mutant *RgCBM40* R128A/R204A to
369 3'SL. The methyl of the N-acetyl moiety and the C-H face of the glycerol moiety reside on a
370 hydrophobic twisted platform surface formed by primarily aromatic residues, of which Tyr116
371 and Tyr210 are essential for binding. Glu126 was also shown to be essential, as predicted
372 given its conservation and interactions with both the N-acetyl group N and the C4 hydroxyl of
373 the sialic acid moiety.

374 *RgCBM40* showed broad specificity for sialylated oligosaccharides with dissociation
375 constants to 3'SL and 6'SL in the millimolar affinity range, 0.57 mM and 1.70 mM,
376 respectively. This is comparable to the affinity recently measured for the isolated *S.*
377 *pneumoniae* SpCBM40_NanC³⁷ against 3'SL (K_d ~ 1.5 mM) and 6'SL (K_d ~ 1.6 mM). Low
378 sialic acid affinity has also been proposed for CpCBM40_NanJ from the *C. perfringens*
379 sialidase however this was not quantified²⁵. Micromolar sialic acid affinity has been observed
380 for *C. perfringens* CpCBM40_NanI and *S. pneumoniae* SpCBM40_NanA^{32,35}. Additional
381 electrostatic interactions with the sialic acid glycerol moiety may contribute to these unusual
382 affinities, in the case SpCBM40_NanA via the introduction of a tryptophan in place of
383 *RgCBM40* Tyr210 (**Supplementary Fig. 3a, b**), and in the case of CpCBM40_NanI via
384 Asn158, which approaches the binding site from a nearby loop extension (**Supplementary**
385 **Fig. 3c**). CpCBM40_NanI also introduces additional water mediated interactions with the
386 galactose residues of bound 3'SL via a further loop extension (**Supplementary Fig. 1h**):
387 These are proposed to provide specificity for the corresponding sialic acid linkage³². A
388 corresponding extension is absent in *RgCBM40* leading to minimal observed interactions
389 between the protein and galactose (**Fig.1f, g, Supplementary Fig 1a**). Similar absence in
390 SpCBM40_NanA suggests that these water-mediated interactions are not the defining
391 feature of high CBM40 sialic acid affinity.

392 Overall the binding epitopes of 3'SL and 6'SL, as determined by STD NMR, were in
393 agreement with the crystal structure, and confirmed the flexibility of the galactose and
394 glucose rings at the reducing end. Although the sialic acid moiety was the main recognition
395 element for the interaction with *RgCBM40*, only weak binding was observed to Neu5Ac or
396 Neu5Gc monosaccharides. Sialic acid residues present in oligosaccharides are α -anomers.
397 However, in solution sialic acid adopts both α and β -anomeric configurations, as well as an
398 open chain conformation, with the β -anomer forming the dominant constituent⁴⁵. In the
399 *RgCBM40* complex crystal structures, sialic acid is bound in the α -anomeric conformation,

400 allowing the axial C2 carboxylic acid moiety to form a conserved interaction with Arg204.
401 The *RgCBM40* preference for the minority α -anomer will incur a large entropic penalty. This
402 may provide a major contributory factor to the low observed monosaccharide affinity.
403 Thermodynamic analysis showed that the reaction is driven by enthalpy, with unfavorable
404 entropy (**Supplementary Table 2**), which is typical of interactions between CBMs and
405 saccharides⁴⁶.

406 The binding specificity of CBMs most commonly matches that of the appended catalytic
407 module^{26,47}. We previously showed that the catalytic activity of *RgNanH* is specific for α 2-3-
408 linked sialic acid³⁰. However, our glycan array and STD NMR data clearly showed that
409 *RgCBM40* can recognize a wide range of α 2-3- and α 2-6-sialic acid-linked oligosaccharides
410 which are commonly found in human GI mucins^{12,21,23}, suggesting an additional function.
411 More than 100 complex oligosaccharides were identified in mucins from human colonic
412 biopsies where most were mono-, di- or trisialylated²³. *RgCBM40* bound Neu5Ac α 2-6Tn and
413 Neu5,9Ac₂ α 2-6Tn, Neu5Ac α 2-3TF and Neu5,9Ac₂-TF9Ac₂ α 2-3TF *but* not to the non-
414 sialylated forms; it also recognises Neu5Ac and acetylated Neu5Ac-linked Lac with α 2-3 and
415 α 2-6 linkage but shows a strict preference for Neu5Ac-linked LacNAc with α 2-3 linkage, in
416 line with the increased expression of group Sd(a)/Cad related epitopes GalNAc β 1-
417 4(NeuAc α 2-3)Gal along the length of the colon¹². Despite the large diversity of structures,
418 the sigmoid MUC2 O-glycan repertoire and relative amounts in normal individuals is
419 relatively constant²³, suggesting their role in selecting a specific mucus-associated
420 microbiota. Many bacterial species bind host tissues through protein-carbohydrate
421 interactions *via* a variety of cell-surface proteins and appendages. Although a wide number
422 of microbial lectins have been functionally and structurally characterized to date, especially
423 from pathogens, only a few carbohydrate-binding proteins present in gut bacteria which
424 interact with mucus have been structurally characterized^{13,15}. Interactions between bacterial
425 adhesins from gut commensals and mucin glycans are generally of low affinity, in line with
426 the localization of these bacteria within the outer mucus layer^{48,49}. Here we showed that
427 *RgCBM40* could recognize mucins with binding affinity increasing with sialic acid level.
428 Binding was highest towards human colonic MUC2, consistent with the increasing sialic acid
429 gradient along the GI tract from the small intestine to the colon in humans²¹. This study
430 demonstrates CBM40 mediating interaction to mucus, therefore expanding the repertoire of
431 bacterial adhesins to mucus. In addition to variations along the length of the GI tract, mucin
432 sialylation varies significantly between species, and thus could influence host species and
433 niche specificity of the gut symbionts. Interestingly, *RgCBM40* also showed binding to
434 Neu5Gc-containing oligosaccharides, albeit to lower affinity as compared to Neu5Ac-
435 oligosaccharides. Humans express predominantly Neu5Ac whereas Neu5Gc is expressed in

436 many non-human mammals⁵⁰. Therefore, the ability of CBM from human gut commensal
437 bacteria to bind to Neu5Gc was unexpected. However, it cannot be excluded that *RgCBM40*
438 mediates binding to dietary Neu5Gc-containing glycoproteins⁵¹.

439 CBMs typically function to maintain carbohydrate-active enzymes (CAZymes) in proximity of
440 the substrate, thereby enhancing catalytic activity^{26,46,52,53}. It has recently been suggested
441 that CBMs may play an additional role in the host–bacterium interaction by not only
442 mediating the attachment of CAZymes to glycans present on host tissues but by aiding the
443 adherence of the entire bacterium²⁷. This would be particularly relevant to bacteria of the
444 human gut microbiota which are characterized by their large and diverse repertoires of CBM-
445 containing CAZymes⁵⁴. Many CAZymes are known, or postulated to be, attached to the
446 bacterial cell surface⁴. Here, immunogold labeling confirmed the presence of *RgNanH* on *R.*
447 *gnavus* ATCC 29149 cell-surface but not on *R. gnavus* E1. In addition, we showed that the
448 binding of *R. gnavus* ATCC 29149 to intestinal mucus was sialic acid mediated. The
449 potential avidity effect of CBM40-mediated binding of sialylated mucins *in vivo* (when
450 naturally present on the bacterial cell surface), may favor a mechanism by which CBM40
451 helps targeting the bacteria towards sialic acid rich regions of the GI tract, therefore
452 promoting bacterial colonization within the outer mucus layer. Our bioinformatics analyses of
453 bacterial genomes showed that *RgCBM40* canonical type domains are widespread among
454 Firmicutes, also reflecting the strong difference in CAZyme content and diversity between
455 the Firmicutes and Bacteroidetes phyla⁵⁴. We thus propose a new role of CBMs in assisting
456 the tropism and spatial distribution of symbiotic bacteria among physical niches in the gut.
457
458

459 **Methods**

460

461 **Materials**

462 General chemicals including Neu5Ac were from Sigma (St Louis/MOI, US). Neu5Gc α 2-3Lac
463 Neu5Gc α 2-6Lac, Neu5Ac-STn, Neu5Gc-STn and STF α OC3H6N3) were synthesised
464 following published methodology^{38,55}. Neu5Gc, 3'SL, 6'SL, 3'SGal, 6'SGal, 3'SLN, 6'SLN,
465 were from Carbosynth. 2,7-anhydro-Neu5Ac was synthesised as previously reported³¹.
466 Sialidase from *Clostridium perfringens* and *Salmonella typhimurium* LT2 were from New
467 England Biolabs (Ipswich, MA US). Sialidase 0625 from *Akkermansia muciniphila* was a gift
468 from WM de Vos³⁰. Polyclonal antiserum against IMAC-purified His₆-RgNanH³⁰ was raised in
469 rabbits by BioGenes GmbH (Berlin, Germany) and provided at a titre of >1:200 000.
470 Protease inhibitors benzamidine, N-ethylmaleimide, PMSF, sodium azide and soy bean
471 inhibitor were from Sigma. Fluorescein labelled *Sambucus nigra* lectin (SNA-FITC)
472 biotinylated SNA (SNA-biotin) and Vectashield were from Vector laboratories (Peterborough,
473 UK). Streptavidin Alexa Fluor 488 conjugate was Thermo Fischer Scientific (Eugene/OR,
474 US). Deuterium oxide (99.9% 2H) and Tris(hydroxymethyl-d3)amino-d2-methane (Tris-d11,
475 98% 2H) were from Sigma. Mouse monoclonal anti-His-HiLyte Flour 555 antibody was
476 obtained from LifeSpan BioSciences (Seattle/WA, US). Blocking reagent was from Perkin
477 Elmer (Boston/MA, US). Rabbit Mucin 2 antibody H-300 was from Santa Cruz (Dallas/TX,
478 US, SC-15334), Goat anti-Rabbit IgG Secondary Antibody, Alexa Fluor 488 (A11034) and
479 Goat anti-Rabbit IgG Secondary Antibody Alexa Fluor 594 (A11037) from Thermo Fischer
480 Scientific. DAPI was from Life Technologies, O.C.T. Compound from VWR and Hydromount
481 from National Diagnostics (Atlanta/GA, USA).

482

483 **Expression and purification of RgCBM40 and RgNanH**

484 Using the full-length sequence encoding RgNanH in pOPINF from *R. gnavus* strain ATCC
485 29149 as a template³⁰, RgCBM40 (residues 50–237), RgNanH (residues 26–723) and
486 RgGH33 (residues 243–723) were cloned into the pEHISTEV vector⁵⁶ using the primers
487 listed in **Supplementary Table 4**. Protein expression and purification of RgCBM40 and
488 RgNanH was similar to that of RgGH33³⁰. Points of divergence are indicated below. For
489 protein expression, recombinant plasmids were transformed into *E. coli* BL21 Rosetta (DE3)
490 (Novagen, NJ, US). A single colony was used to inoculate a 10 ml Luria Bertani (LB)
491 medium pre-culture, which was incubated overnight under shaking at 200 rpm (at 30 °C for
492 crystallisation and protein size determination or at 37 °C for all other protein assays). The
493 pre-culture was used to inoculate 500 ml of auto induction medium (Formedium, Norfolk,
494 UK), which was incubated under shaking at 37 °C for 3 h followed by 60 h incubation at 16
495 °C. All cultures were inoculated with 50 µg ml⁻¹ kanamycin.

496 For crystallisation and protein size determination, cells were harvested by centrifugation,
497 resuspended in phosphate buffered saline (PBS, 150 mM sodium chloride, 10 mM sodium
498 phosphate, pH 7.4) for *RgCBM40* and in 20 mM Tris-HCl pH 7.5, 50 mM NaCl for *RgNanH*,
499 supplemented with DNase I (20 µg ml⁻¹) and cOmplete protease inhibitor mixture tablets
500 (Roche, Welwyn Garden City, UK), and lysed using a constant flow cell disrupter. Insoluble
501 components were removed by centrifugation and filtration through a 0.22 µm pore size
502 syringe driven filter (Millipore, NJ, US). Soluble lysate was loaded onto a nickel-Sepharose
503 column (GE Healthcare, Little Chalfont, UK) overnight at 4 °C. The sample was then washed
504 extensively with lysis buffer supplemented with 5 mM imidazole for *RgCBM40* and with
505 150 mM imidazole for *RgNanH* and was eluted using lysis buffer supplemented with 50 mM
506 imidazole for *RgCBM40* and with 300 mM imidazole for *RgNanH*. The sample was then
507 dialysed into lysis buffer and cleaved of its six-histidine tag using Tobacco Etch Protease at
508 a mass ratio of 1:50 overnight at 4 °C. Finally, the gel filtration step using a Sephacryl S-100
509 column (GE Healthcare) was performed using 20 Tris pH 7.5 with 50 mM NaCl. The purified
510 *RgCBM40* was crystallised as described below. To determine the size in solution of
511 *RgNanH*, size exclusion chromatography with multi angle light scattering (SEC-MALS) was
512 performed using an NGC chromatography system (Biorad, Hercules, CA,US) equipped with
513 a DAWN HELEOS II MALS detector (Wyatt technology, Haverhill, UK) and an Optilab T-rEX
514 differential Refractive Index detector (Wyatt Technology). The data were analysed using
515 ASTRA (Wyatt Technology).

516 For all other protein assays, the cell pellets were resuspended in Bug buster-HT (Merck,
517 Kenilworth, NJ, US) with the supplied lysozyme and lysed by shaking in this solution for 1 h
518 at room temperature. Insoluble material was removed by centrifugation at 4 °C, 3320 g for
519 25 min and the supernatant was dialysed into desalting buffer (50 mM Tris-HCl, 150 mM
520 NaCl, pH 7.8 containing 10 mM imidazole for *RgGH33* and *RgNanH* and no imidazole for
521 *RgCBM40*, the difference is due to the poor binding of the His₆-tag of *RgCBM40* to the nickel
522 column) to remove the Bug buster-HT. Again insoluble material was removed by
523 centrifugation as above, except at 8 000 g. Purification of the soluble lysate was loaded onto
524 the immobilized metal ion affinity chromatography (IMAC column, His-bind, Novagen) in
525 binding buffer (desalting buffer with the addition of 10 mM imidazole) using the Akta Express
526 (GE Healthcare). The protein was eluted with binding buffer containing 500 mM imidazole
527 and then immediately desalted into desalting buffer. The partially purified protein was
528 concentrated using 3.5 kDa MWCO spin columns (Sartorius, Gottingen, Germany) prior to
529 gel filtration again with the Akta Express in desalting buffer (see above) on a Superdex 75
530 column (GE Healthcare). Purity of the proteins was assessed throughout by SDS-PAGE
531 using the Novex system (Thermo Fisher Scientific).

532

533 **Site-directed mutagenesis**

534 Site directed mutagenesis of *RgGH33* to introduce the D282A mutation in the active site was
535 carried out using the QuikChange kit, following the manufacturer's instructions, Agilent
536 (Santa Clara, CA, US). Site-directed mutants of *RgCBM40*; I95A, Y116A, E126A, R128A,
537 R204A and double mutant R128A/R204A, were obtained from NZyTech (Lisbon, Portugal).
538 The primers are listed in **Supplementary Table 4**. The integrity of the *RgGH33* and
539 *RgCBM40* mutants was checked by circular dichroism (CD).

540

541 **Circular dichroism**

542 CD spectra were recorded using a JASCO J-700 spectropolarimeter, under the following
543 conditions: 20 nm/min scan speed, bandwidth 1 nm, response 2 s, 5 points/nm and 4
544 accumulations. Far-UV spectra (260-180nm) were recorded in a 0.1 mm pathlength cell. The
545 spectropolarimeter was calibrated using camphorsulphonic acid (Sigma). The protein was
546 extensively dialysed into 10 mM sodium phosphate buffer, pH 6.5 and a buffer only control
547 was subtracted from all spectra using the molar CD factor calculated as follows: $(113 \times 30 \times$
548 $10^{-6}) / [\text{conc}(\text{mg ml}^{-1}) \times \text{pathlength}(\text{cm})]$.

549

550 **Protein crystallisation**

551 The final crystallisation condition was 0.2 M ammonium chloride with 20% PEG 8000. The
552 drop contained 0.5 μl protein solution at 25 mg ml^{-1} and 0.5 μl reservoir solution, initial
553 crystals grew in four weeks and growth time was improved significantly using micro
554 seeding⁵⁷. Crystals were cryoprotected using the crystallisation condition supplemented with
555 25% (w/w) glycerol. To achieve crystal structures in complex with 3'SL and 6'SL the crystals
556 were grown in crystallisation condition supplemented with 20 mM ligand followed by a 60
557 min soak in crystallisation condition supplemented with 100 mM ligand immediately prior to
558 cryoprotection and mounting.

559

560 **Solving the crystal structure**

561 X-ray diffraction experiments were performed at 100 K. Data were collected using a Rigaku
562 MSC Micromax 007 HF X-ray source, with a fixed wavelength of 1.542 Å, and a Saturn 944+
563 CCD detector. Sweeps were indexed and integrated separately and then scaled together
564 within the HKL2000 data processing package⁵⁸. Phasing was performed by Phaser⁵⁹ within
565 the CCP4 package⁶⁰ using the CBM40 of the *M. decora* sialidase NanL (*MdCBM40_NanL*)
566 (PDB 2SLI)³³ as the molecular replacement model. The model was refined using iterative
567 cycles of Refmac⁶¹ and Coot⁶². The PDB REDO server was used to optimize the
568 refinement parameters⁶³. The model was validated using the Molprobit server⁶⁴. Paired

569 refinement performed by the PDB REDO server indicated that the models were improved by
570 the inclusion of high resolution, low completeness data for the 3'SL and 6'SL complexes⁶⁵.
571 For an illustrative stereo image of a portion of the electron density map, see **Supplementary**
572 **Fig. 13**.

573

574 **Isothermal titration calorimetry**

575 ITC experiments were performed using the PEAQ-ITC system (Malvern, Malvern, UK) with a
576 cell volume of 200 μ l. Prior to titration protein samples were exhaustively dialyzed into PBS.
577 The ligand was dissolved in the dialysis buffer. The cell protein concentration was 115 μ M
578 (except for mutant I95A where it was 173 μ M and the wild type interaction with 6'SL where it
579 was 230 μ M) and the syringe ligand concentration was 10 mM (25 mM for Neu5Ac).
580 Controls with titrant (sugar) injected into buffer only were subtracted from the data. Analysis
581 was performed using Malvern software, using a single binding site model. The stoichiometry
582 of binding sites was set to 1.0 as this was evident from the crystal structure. Quantitative and
583 most qualitative experiments were carried out in triplicate.

584

585 **STD NMR experiments**

586 ¹H and ¹³C resonance assignment for all the sugars was performed on the bases of 1D ¹H,
587 2D DQF-COSY, TOCSY, HSQC and NOESY experiments run on the free ligands in
588 unbuffered D₂O, pH 7.0. For STD NMR experiments, all the samples consisted of 1 mM
589 sialoglycans and 50 μ M RgCBM40 (WT or I95A mutant) in D₂O buffer solution of 10 mM
590 Tris-d₁₁, pH 7.8 and 100 mM NaCl (ligand : protein ratio 20 : 1). An STD pulse sequence that
591 included 2.5 ms and 5 ms trim pulses and a 3 ms spoil gradient was used. Saturation was
592 achieved applying a train of 50 ms Gaussian pulses (0.40 mW) on the f2 channel, at 0.60
593 ppm (on-resonance experiments) and 40 ppm (off-resonance experiments). The broad
594 protein signals were removed using a 40 ms spinlock (T1 ρ) filter. All the experiments were
595 recorded at ¹H frequency of 800.23 MHz on a Bruker Avance III spectrometer equipped with
596 a 5 mm probe TXI 800 MHz H-C/N-D-05 Z BTO, at 288 K. For all the sialoglycans in the
597 presence of RgCBM40, an STD experiment with a saturation time of 2 s and a relaxation
598 delay of 5 s was performed, as a first test for binding. For the confirmed binders, the STD
599 NMR experiments were carried out at different saturation times (0.5, 1, 2, 3, 4 and 5 s) with
600 1K scans and relaxation delay of 5 s, in order to obtain the binding epitope mapping. The
601 resulting build-up curves for each proton were fitted mathematically to a mono-exponential
602 equation ($y=a*[1-\exp(b*x)]$), from which the initial slopes ($a*b$) were obtained. For each
603 ligand, the binding epitope mapping was obtained by dividing the initial slopes by the one of
604 the H7 proton of the corresponding sialic acid ring, to which an arbitrary value of 100% was
605 assigned. This normalization of the STD values allows the comparison across all the

606 sialoglycans.

607

608 **Structure-based sequence alignment and bioinformatics analyses**

609 A structural alignment of *Rg*CBM40 was carried out with all CBM40 structures available to
610 date (see Results and **Supplementary Methods**). This served as a basis for producing an
611 alignment including both canonical and *Vibrio* type CBM40 sequences to create a profile
612 Hidden Markov Model (pHMM) using the HMMER3 software (<http://hmmer.org/>)
613 (**Supplementary Fig. 14**), intended to detect both types simultaneously and ensure that hit
614 sequences of both types are thus properly aligned for subsequent comparative analysis.
615 Additionally, we created pHMMs corresponding to the canonical-only and *Vibrio* type-only
616 CBM40 sequences of this alignment, to resolve the type of each hit. Protein domain
617 databases such as Pfam⁶⁶ currently characterize the canonical CBM40 as a sequence family
618 belonging to a larger superfamily ("clan"), and some individual domains make good matches
619 to more than one related family, i.e. including non-CBM40 such as "Concanavalin A-like
620 lectin/glucanases" (in contrast, no Pfam domain clearly defines the *Vibrio* CBM40). We
621 therefore also used the corresponding Pfam pHMMs, as well as our own, to search all
622 available (177 million) protein sequences from annotated NCBI prokaryote genomes, using
623 HMMER3. Where individual hit domains matched multiple pHMMs, we compared scores to
624 identify and discard hits which might be better regarded as related, non-CBM40 domains.
625 The remaining CBM40 proteins were screened for the presence of the sialidase domain
626 (GH33) and IT-sialidase, as previously described³⁰. We reduced this to a nonredundant set
627 (**Supplementary Methods**) for further analysis. A detailed phylogenetic analysis is beyond
628 the scope of this study, but we estimated evolutionary distances between these 51
629 representative sequences using fprotdist in EMBASSY-PHYLIP^{67,68} from which the tree was
630 calculated by neighbour-joining (fneighbor). All sites were included in the analysis, using the
631 PMB model with a uniform rate of evolution. This was repeated on 1,000 replicate datasets
632 produced by bootstrap resampling (fseqboot; consensus tree produced by fconsense). The
633 figure was produced with FigTree (<http://tree.bio.ed.ac.uk/software/figtree/>). Bioinformatics
634 analyses were performed using the Gut Health and Food Safety Linux servers at Quadram
635 Institute Bioscience.

636

637 **Glycan microarray screening**

638 Glycan microarrays were fabricated using epoxide-derivatized slides as previously described
639 (38). Printed glycan microarray slides were blocked by ethanolamine, washed and dried.
640 Slides were then fitted in a multi-well microarray hybridization cassette (AHC4X8S, ArrayIt,
641 Sunnyvale, CA, USA) to divide into 8 subarrays. The subarrays were blocked with ovalbumin
642 (1% w/v) in PBS (pH 7.4) for 1 h at room temperature, with gentle shaking. Subsequently,

643 the blocking solution was removed and diluted protein samples of *RgCBM40* and *RgGH33*
644 D282A with various concentrations were added to each subarray. After incubating the
645 samples for 2 h at room temperature with gentle shaking, the slides were washed. Diluted
646 anti-His-HiLyte Flour 555 antibodies in PBS were added to the subarrays, incubated for 1 h
647 at room temperature, washed and dried. The microarray slides were scanned by Genepix
648 4000B microarray scanner (Molecular Devices Corp., Union City, CA, USA). Data analysis
649 was performed using Genepix Pro 7.0 analysis software (Molecular Devices Corp.). It is
650 important to note that glycans on the array with sialic acid O-acetyl groups undergo gradual
651 losses of these labile ester groups. Therefore, definitive conclusions about 9-O-acetylation
652 are only possible in instances wherein binding is exclusively to the O-acetylated sialoglycan
653 spot, and not to the corresponding non-O-acetylated spot.

654

655 ***RgCBM40* binding to mucus-producing cells**

656 The binding of *RgCBM40* to mucus-producing LS174T cell line (80% confluent, passage 12)
657 was performed by incubating the cells with $150 \mu\text{g ml}^{-1}$ *RgCBM40* in cell culture medium for
658 2 h at 37 °C. Control samples were incubated with cell culture medium only. The cells were
659 then washed with PBS, fixed in methacarn (60% dry methanol, 30% chloroform and 10%
660 acetic acid) and washed in PBS containing 0.05% bovine serum albumin (BSA). Blocking
661 was done with TNB buffer (0.5% w/v blocking reagent in 100 mM Tris-HCl pH 7.5, 150 mM
662 NaCl) supplemented with 5% goat serum. The *RgCBM40* binding was detected with custom-
663 made rabbit *RgNanH* antiserum diluted 1:100 in PBS and goat anti-rabbit antibody diluted
664 1:400 in PBS. The same antibodies were used for negative control sample (*RgCBM40*-free).
665 In the lectin control sample, SNA-biotin (incubated at $75 \mu\text{g ml}^{-1}$) was detected with
666 streptavidin conjugate ($2.5 \mu\text{g ml}^{-1}$). MUC2 was detected with rabbit Mucin 2 antibody diluted
667 1:50 in PBS and goat anti-rabbit antibody diluted 1:200 in PBS. The cells were
668 counterstained with DAPI and mounted in Vectashield. The slides were imaged using a
669 Zeiss Axio Imager 2 microscope.

670

671 ***RgCBM40* and *R. gnavus* binding to intestinal tissue**

672 To assess the binding of *RgCBM40* to intestinal tissue sections, colon of wild type C57BL/6
673 mouse was washed with PBS, fixed in methacarn, embedded in O.C.T. compound and cut
674 into 8 μm sections. Access to mouse tissues was carried out under the Animal Welfare and
675 Ethical Review Body of University of East Anglia's establishment licence (according to Home
676 Office requirements). Tissue sections were washed in PBS containing 0.05% BSA and
677 blocked with TNB buffer (0.5% w/v blocking reagent in 100 mM Tris-HCl pH 7.5, 150 mM
678 NaCl) supplemented with 5% goat serum. The slides were then washed in PBS 0.05% BSA,
679 followed by 2 h incubation of $150 \mu\text{g ml}^{-1}$ *RgCBM40* in PBS at 37 °C. Control tissue sections

680 were incubated in PBS only. After washes in PBS with 0.05% BSA, the binding of *RgCBM40*
681 was detected with custom-made rabbit *RgNanH* antiserum (diluted 1:100 in TNB buffer) and
682 goat anti-rabbit antibodies (diluted 1:200 in PBS). Negative control sample (*RgCBM40*-free)
683 was also incubated with these primary and secondary antibodies. Muc2 was detected with
684 Mucin 2 antibody diluted 1:100 in TNB buffer and goat-anti rabbit antibody diluted 1:200 in
685 PBS. In lectin controls SNA-FITC was incubated at 4 $\mu\text{g ml}^{-1}$. The sections were
686 counterstained with DAPI and mounted in Hydromount mounting medium. The slides were
687 imaged using Zeiss an Axio Imager 2 microscope. To assess the binding specificity of
688 *RgCBM40* to sialylated structures, the tissue sections were pre-treated with sialidase.
689 Briefly, saponification was performed to make the enzymatic digestion of mouse colonic
690 tissue sections effective⁶⁹. The sections were treated with 0.5% KOH in 70% ethanol for 15
691 min at room temperature. After three PBS washes, 500 U ml^{-1} sialidase from *Clostridium*
692 *perfringens* in GlycoBuffer 1 (New England Biolabs) was added and incubated for 14 h at 37
693 °C. Sections were incubated in sialidase-free GlycoBuffer 1 under the same experimental
694 conditions and used as a control of sialidase digestion to assess the binding *RgCBM40* and
695 SNA to tissue sections as described above.

696 To assess the binding of *R. gnavus* to intestinal tissue sections, colon of wild type C57BL/6
697 mouse was washed with PBS, fixed in methacarn, embedded in O.C.T. compound and cut
698 into 12 μm sections. Tissue sections were washed in PBS, then incubated with SNA in PBS
699 at 20 $\mu\text{g ml}^{-1}$ for 1 h. Prior to incubation with bacteria, the slides were washed with PBS. *R.*
700 *gnavus* ATCC 29149 was cultured anaerobically in BHI-YH media for 24 h as previously
701 described²⁹. The culture was then then used to inoculate YCFA media supplemented with
702 3'SL at a concentration of 7 mg ml^{-1} , and cultured for 20 h. The bacteria were then washed
703 twice with fresh YCFA, and resuspended at an OD of 1. The tissue sections were then
704 transferred in a humid chamber to the anaerobic cabinet, and the bacteria incubated on the
705 sections for 1 h at 37°C. The slides were then washed twice with YCFA and fixed with 4%
706 paraformaldehyde in PBS for 15 min. The slides were transferred out of the anaerobic
707 cabinet, then washed with PBS and blocked with TNB buffer (0.5% w/v blocking reagent in
708 100 mM Tris-HCl pH 7.5, 150 mM NaCl) supplemented with 5% goat serum. The presence
709 of *R. gnavus* and Muc2 was detected with custom-made rabbit *RgNanH* antiserum (diluted
710 1:100) and Mucin 2 antibody (1:100), respectively. Goat anti-rabbit antibodies (diluted 1:500)
711 were used for immunodetection. The sections were counterstained with DAPI and mounted
712 in Prolong gold anti-fade mounting medium. The slides were imaged using Zeiss an Axio
713 Imager 2 microscope, using a x63 objective.

714

715 **Mucin purification**

716 Culture media from LS174T cell line were freeze-dried before extraction of MUC2. After
717 freeze-drying, samples were solubilised overnight in 6 M guanidine chloride (GuCl) buffer
718 containing protease inhibitors (7.95 mM EDTA, 12.25 mM benzamidine, 6.25 mM *N*-
719 ethylmaleimide, 1.25 mM PMSF, 3.75 mM sodium azide, 0.1 mg/ml soy bean inhibitor).
720 Samples were centrifuged at 18 500 *g*. The pellet was reduced with dithiothreitol (DTT) at 10
721 mM for 4 h at 45 °C and alkylated with 25 mM iodoacetamide overnight before dialysis
722 against 50 mM ammonium bicarbonate. The same protocol was followed for purifying
723 mucins from the scraped mucus from small intestine and colon of mouse models. The
724 supernatants containing soluble mucins were diluted in 4 M guanidinium chloride (GuCl) with
725 phosphate buffered saline (PBS) and adjusted with cesium chloride at 1.4 g ml⁻¹ density.
726 Supernatants were subjected to an ultracentrifugation (Beckman, Brea, US) at 234 000 *g* for
727 72 h at 20 °C. Fractions of 1 ml were collected and weighed. Fractions between 1.35 and
728 1.45 g ml⁻¹ were kept and dialysed against 50 mM ammonium bicarbonate. These fractions
729 contained the purified mucins.

730

731 **Release of oligosaccharides from mucin**

732 The mucins were subjected to β-elimination under reductive conditions (0.1 M sodium
733 hydroxide, 1 M sodium borohydride) for 20 h at 45 °C. The reaction was stopped by adding
734 Dowex 50 x 8 (Sigma) and filtered before being co-evaporated with methanol 3 times.
735 Remaining salts were removed by Carbohydrate (Grace, Columbia, US).

736

737 **Permethylation of O-glycans**

738 Permethylation was performed on released O-glycans from the different mucins samples.
739 Samples were solubilized in 200 μl dimethyl sulfoxide. Then sodium hydroxide (trace of
740 powder) and 300 μl iodomethane were added in anhydrous conditions and the samples
741 vigorously shaken at room temperature for 90 min. The permethylation reaction was stopped
742 by addition of 1 ml acetic acid (5% vol/vol). Permethylated O-glycans were purified on a
743 Hydrophilic-Lipophilic Balanced (HLB) Oasis cartridge (Waters, Milford, US). Briefly,
744 cartridges were activated by methanol, equilibrated with methanol:water (5:95, vol:vol), and
745 samples loaded onto the cartridges. Cartridges were washed by methanol:water (5:95,
746 vol:vol) and the permethylated O-glycans eluted by methanol.

747

748 **Analysis of permethylated O-glycans by mass spectrometry**

749 MALDI-TOF and TOF/TOF-MS data were acquired using the Bruker Autoflex analyzer mass
750 spectrometer (Applied Biosystems, Foster City, CA, US) in the positive-ion and reflectron
751 mode by using 2,5-dihydroxybenzoic acid (DHB; Sigma; 10 mg ml⁻¹ in 70:30 methanol:water)
752 as the matrix. The relative quantification of sialylation on mucins was calculated based on

753 the sum of all areas of mass peaks corresponding to sialylated structures divided by the sum
754 of all areas of mass peaks corresponding to defined O-glycans.

755

756 **Enzyme Linked Immunosorbent Assay**

757 *RgCBM40* binding to purified mucins was tested by ELISA. Mucins (100 μl of 10 $\mu\text{g ml}^{-1}$)
758 were immobilised onto a high binding 96 well plate (Greiner, Stonehouse, UK) overnight at 4
759 $^{\circ}\text{C}$. All subsequent steps were carried out for 1 h at room temperature. The plates were
760 blocked with 3% (w/v) BSA, incubated with *RgCBM40* (500 $\mu\text{g ml}^{-1}$), followed by an
761 incubation with 1:5 000 anti-*RgNanH* (raised in rabbit, Biogenes) then with 1:5 000 anti-
762 rabbit secondary antibody (raised in donkey) conjugated to peroxidase (GE Healthcare).
763 Between each step the plate was washed with 3 x 300 μl of PBS containing 0.05% (v/v)
764 Tween 20 (PBST). Prior to detection, an additional wash step and 30 sec incubation with
765 PBST was carried out. Binding was detected using tetramethylbenzidine (TMB) visualisation
766 solution (Biolegend, San Diego, CA, US) which was incubated for 15 min. The reaction was
767 stopped by addition of 2 M H_2SO_4 and absorbance measured at 450 nm using a plate-reader
768 (Bench Marl Plus, Biorad), subtracting background readings at 570 nm. Negative controls
769 including no *RgCBM40* (subtracted from A_{450} value), no primary or no secondary antibody
770 were carried out in parallel. For comparison between plates, values were normalised to the
771 reading for LS174T MUC2 which was arbitrarily set at 100%. For enzymatic treatment of the
772 mucin, LS174T MUC2 (2 mg ml^{-1}) was incubated with sialidases (2 $\mu\text{g ml}^{-1}$) overnight at 4 $^{\circ}\text{C}$
773 on a rotary wheel prior to immobilization on the plate. For chemical treatment of mucin,
774 LS174T MUC2 was incubated with 0.1 M trifluoroacetic acid (TFA) at 80 $^{\circ}\text{C}$ for 1 h, dialysed
775 against ammonium bicarbonate (50 mM), lyophilised and redissolved in H_2O . For the
776 competition assays, *RgCBM40* was incubated with 1 mM of free sugar overnight at 4 $^{\circ}\text{C}$ on a
777 rotary wheel prior to addition to the ELISA plate as above. Experiments were carried out in
778 triplicate.

779

780 **HPAEC-PAD analyses**

781 The substrates, 3'SL (500 μM , 8.5 nM enzyme), 3'SLX (Neu5Ac form), 500 μM , 80 nM
782 enzyme) or LS174T MUC2 (0.9 mg ml^{-1} , 1.5 nM enzyme) were incubated with *RgNanH* or
783 *RgGH33* at 37 $^{\circ}\text{C}$ in 20 mM sodium phosphate buffer, pH 6.5. BSA (0.1 mg ml^{-1}) was
784 included in the oligosaccharide reactions. Control reactions without enzyme were also
785 carried out in parallel. Aliquots of reaction were removed and the reaction terminated by
786 boiling for 20 min. For LS174T MUC2, the released sugars were removed using 5 kDa
787 MWCO spin columns and the remaining mucin subjected to acid hydrolysis; the samples
788 were incubated with 0.1 M HCl at 80 $^{\circ}\text{C}$ for 1 h, dried under vacuum and resuspended in

789 H₂O at 1 mg ml⁻¹. The amount of Neu5Ac remaining on the mucin was quantified by
790 comparing the peak size for Neu5Ac with an internal standard of 2-keto-3-deoxynononic acid
791 (Kdn). The reaction products for all substrates were filtered with 0.22 µm spin tubes prior to
792 analysis by HPAEC-PAD (Dionex ICS-5000, Thermo Fisher Scientific). An internal standard
793 of fucose (50 µM) was used for 3'SL and 3'SLX. For 3'SL, a Carbo-Pac PA1 column
794 (Thermo Fisher Scientific) was used with a 6 min isocratic gradient of 100 mM sodium
795 hydroxide, 100 mM sodium acetate followed by a 10 min washing step with 100 mM sodium
796 hydroxide, 200 mM sodium acetate and 10 min re-equilibration with 100 mM sodium
797 hydroxide, 100 mM sodium acetate. For 3'SLX, a Carbo-Pac PA100 was used with 5 min at
798 100 mM sodium hydroxide, a gradient of 0–50 mM sodium acetate over 5 min, followed by a
799 gradient of 50–225 mM sodium acetate. The column was then cleaned with 500 mM sodium
800 acetate for 5 min and re-equilibrated for 15 min at 100 mM sodium hydroxide. For analysis of
801 the acid hydrolysis products of MUC2, a Carbo-Pac PA10 was used with a gradient of 70–
802 300 mM sodium acetate with 100 mM sodium hydroxide over 10 min, a brief (1 min) period
803 of 300 mM sodium acetate followed by a decrease (over 1 min) to 70 mM sodium acetate
804 and 15 min re-equilibration at 70 mM sodium acetate. All columns were protected with their
805 respective guard columns, except for the mucin analysis where an amino-guard column was
806 used.

807

808 **Western blotting**

809 *R. gnavus* strains were grown to stationary phase and cells pelleted by centrifugation for 10
810 min at 3 000 *g* at 4 °C. The supernatant was collected and the extracellular proteins
811 concentrated 50-fold using a 10-kDa MWCO Amicon Ultra-0.5 Centrifugal Filter (Millipore,
812 Watford, UK). The cell pellet was re-suspended in 20 µl PBS with an equal bead (100 µm
813 glass beads) volume added and samples vortexed at full speed three times for 2 min with 2
814 min rest intervals on ice. The volume was made up to 17 µl per mg wet cell weight with PBS
815 and vortexed at full speed again for 2 min. The beads were removed by allowing them to
816 settle under gravity and the remaining samples centrifuged for 30 min at 17 000 *g* at 4 °C.
817 The supernatant containing the soluble cytosolic proteins was collected and concentrated
818 10-fold using a 10-kDa MWCO Amicon Ultra-0.5 Centrifugal Filter. The remaining pellet was
819 dissolved in 1.7 µl per mg wet cell weight digestion buffer (50 mM Tris-HCl (pH 8.0), 5 mM
820 MgCl₂, 5 mM CaCl₂, 10 mg ml⁻¹ Hen Egg White Lysozyme (Sigma), and incubated at 37°C
821 for 3 h. The samples were centrifuged for 30 min at 17 000 *g* at 4 °C, and the supernatant
822 containing the cell wall associated proteins collected. Samples were analysed on duplicate
823 NuPAGE Novex 4–12% Bis-Tris gels, one gel was stained with InstantBlue stain (Expedeon,
824 Swavesey, UK) and the other gel blotted onto a PVDF membrane using X-cell II Blot module

825 (Thermo Fisher Scientific), according to manufacturer's instructions. Membranes were
826 blocked with 3% BSA in PBST for 3 h, and then incubated with the custom-made anti-
827 *RgNanH* antibody raised in rabbit diluted 1:5000 in 1% BSA in PBST overnight. Blots were
828 washed in PBST, then incubated with anti-rabbit IgG antibody (Sigma) diluted 1:7 500 in 1%
829 BSA in PBST for 2 h. After washing three times in PBST, the blots were incubated using a
830 visualisation solution (10 ml of 0.1 M Tris-HCl (pH 9.6), 40 µl of 1 M MgCl₂, 20 µl of nitroblue
831 tetrazolium, and 10 µl of 5-Bromo-4-Chloro-3-Indolyl phosphate, Sigma) for up to 15 min,
832 and washed in distilled water to stop the development of the signal.

833

834 **Immunogold labelling of whole bacterial cells**

835 *R. gnavus* strains were grown to stationary phase and cells pelleted by centrifugation for 10
836 min at 3 000 *g* at 4 °C before being resuspended in PBS. A small drop of concentrated *R.*
837 *gnavus* cell suspension was applied to a formvar/carbon coated gold TEM grid (Agar
838 Scientific, Stansted, UK) and left for 1 min. The bacteria on the grids were vapour fixed by
839 placing the grids in a sealed Petri dish with a small cap-full of 25% glutaraldehyde (Agar
840 Scientific) for 2 h. The grids were floated on drops of 50 mM Glycine/PBS for 15 min
841 followed by floating on drops of Aurion blocking buffer (Aurion, Wageningen, The
842 Netherlands) for 30 min. The grids were then washed five times for 5 min with 0.1% BSA-C
843 (Aurion) in PBS. Grids were incubated in anti-*RgNanH* antibody raised in rabbit diluted
844 1:2000 with 0.1% BSA-C/PBS or in a control solution of 0.1% BSA-C/PBS overnight at 4°C.
845 The grids were washed five times for 5 min with 0.1% BSA-C/PBS. Grids were then
846 transferred to a 1/50 dilution of goat-anti-rabbit antibody conjugated with 10 nm gold balls
847 (Agar Scientific) in 0.1% BSA-C/PBS and incubated for 2 h at room temperature. The grids
848 were washed five times for 5 min with 0.1% BSA-C/PBS, followed by three 5 min washes in
849 PBS only. The grids were refixed by immersing them in 2% glutaraldehyde/PBS for 1.5 h
850 followed by three 5 min PBS washes and three 5 min distilled water washes before the grids
851 were carefully blotted and dried. The grids were examined and imaged in a FEI Tecnai G2
852 20 Twin transmission electron microscope at 200 kV.

853

854 **Statistical analysis**

855 One-way ANOVA model analyses were used to assess the binding of *RgCBM40* to purified
856 mucins by ELISA. When the effect of the factor was found to be significant (*p* value < 0.05)
857 and its number of levels greater than 2, a Tukey test was used to assess the significance of
858 the difference between multiple means. Statistical analyses were performed using the
859 software SAS 9.4 (NC, USA).

860

861 **Data availability**

862 Atomic coordinates have been deposited in the Protein Data Bank (www.rcsb.org) with
863 accession codes: unbound, 6ER2; 3'SL bound, 6ER3, 6'SL bound; 6ER4. All other relevant
864 data are available from the authors.

865

866

867 **References**

- 868 1. Sekirov, I., Russell, S. L., Antunes, L. C. M. & Finlay, B. B. Gut Microbiota in Health and
869 Disease. *Physiol. Rev.* **90**, 859-904 (2010).
- 870 2. Donaldson, G. P., Lee, S. M., & Mazmanian, S. K. Gut biogeography of the bacterial
871 microbiota. *Nat. Rev. Microbiol.* **14**, 20-32 (2016).
- 872 3. Martens, E. C., Chiang, H. C. & Gordon, J. I. Mucosal glycan foraging enhances fitness
873 and transmission of a saccharolytic human gut bacterial symbiont. *Cell Host Microbe* **4**, 447-
874 457(2008).
- 875 4. Flint, H. J., Scott, K. P., Duncan, S. H., Louis, P. & Forano, E. Microbial degradation of
876 complex carbohydrates in the gut. *Gut Microbes* **3**, 289-306 (2012).
- 877 5. Johansson, M. E. V., Larsson, J. M. H. & Hansson, G. C. The two mucus layers of colon
878 are organized by the MUC2 mucin, whereas the outer layer is a legislator of host-microbial
879 interactions. *Proc. Natl. Acad. Sci. U. S. A.* **108**, 4659-4665 (2011).
- 880 6. McGuckin, M. A., Lindén, S. K., Sutton, P. & Florin, T. H. Mucin dynamics and enteric
881 pathogens. *Nat. Rev. Microbiol.* **9**, 265-278 (2011).
- 882 7. Manichanh, C., Borrueal, N., Casellas, F. & Guarner, F. The gut microbiota in IBD. *Nat.*
883 *Rev. Gastroenterol. Hepatol.* **9**, 599-608 (2012).
- 884 8. Sheng, Y. H., Hasnain, S. Z., Florin, T. H. J. & McGuckin, M. A. Mucins in inflammatory
885 bowel diseases and colorectal cancer. *J. Gastroenterol. Hepatol.* **27**, 28-38 (2012).
- 886 9. Li, H. *et al.* The outer mucus layer hosts a distinct intestinal microbial niche. *Nat.*
887 *Commun.* **6**, 8292 (2015).
- 888 10. Ouwerkerk, J. P., de Vos, W. M. & Belzer, C. Glycobiome: Bacteria and mucus at the
889 epithelial interface. *Best Pract. Res. Clin. Gastroenterol.* **27**, 25-38 (2013).
- 890 11. Jensen, P. H., Kolarich, D. & Packer, N. H. Mucin-type O-glycosylation--putting the
891 pieces together. *FEBS J.* **277**, 81-94 (2010).
- 892 12. Robbe, C., Capon, C., Coddeville, B. & Michalski, J. C. Structural diversity and specific
893 distribution of O-glycans in normal human mucins along the intestinal tract. *Biochem. J.* **384**,
894 307-316 (2004).
- 895 13. Juge, N. Microbial adhesins to gastrointestinal mucus. *Trends Microbiol.* **20**, 30-39
896 (2012).
- 897 14. Tailford, L.E., Crost, E.H., Kavanaugh, D. & Juge, N. Mucin glycan foraging in the human
898 gut microbiome. *Front. Genet.* **6**, 81 (2015).
- 899 15. Etzold, S. & Juge, N. Structural insights into bacterial recognition of intestinal mucins.
900 *Curr. Opin. Struct. Biol.* **28**, 23-31 (2014).
- 901 16. Ng, K. M. *et al.* Microbiota-liberated host sugars facilitate post-antibiotic expansion of
902 enteric pathogens. *Nature* **502**, 96-99 (2013).
- 903 17. Tong, M. *et al.* Reprograming of gut microbiome energy metabolism by the FUT2
904 Crohn's disease risk polymorphism. *ISME J.* **8**, 2193-2206 (2014).

- 905 18. Bergstrom, K. S. & Xia, L. Mucin-type O-glycans and their roles in intestinal
906 homeostasis. *Glycobiology* **23**, 1026-1037 (2013).
- 907 19. Lewis, A. L. & Lewis, W. G. Host sialoglycans and bacterial sialidases: a mucosal
908 perspective. *Cell. Microbiol.* **14**, 1174-1182 (2012).
- 909 20. Juge, N., Tailford, L. & Owen, C. D. Sialidases from gut bacteria: a mini-review.
910 *Biochem. Soc. Trans.* **44**, 166-175 (2016).
- 911 21. Robbe, C. *et al.* Evidence of regio-specific glycosylation in human intestinal mucins:
912 presence of an acidic gradient along the intestinal tract. *J. Biol. Chem.* **278**, 46337-46348.
913 (2003).
- 914 22. Holmén Larsson, J. M., Thomsson, K. A., Rodríguez-Piñeiro, A. M., Karlsson, H. &
915 Hansson, G. C. Studies of mucus in mouse stomach, small intestine, and colon. III.
916 Gastrointestinal Muc5ac and Muc2 mucin O-glycan patterns reveal a regiospecific
917 distribution. *Am. J. Physiol. Gastrointest. Liver Physiol.* **305**, G357-363 (2013).
- 918 23. Larsson, J. M., Karlsson, H., Sjövall, H. & Hansson, G. C. A complex, but uniform O-
919 glycosylation of the human MUC2 mucin from colonic biopsies analyzed by nanoLC/MSn.
920 *Glycobiology* **19**, 756-766 (2009).
- 921 24. Moustafa, I. *et al.* Sialic acid recognition by *Vibrio cholerae* neuraminidase. *J. Biol.*
922 *Chem.* **279**, 40819-40826 (2004).
- 923 25. Boraston, A. B., Ficko-Blean, E. & Healey, M. Carbohydrate recognition by a large
924 sialidase toxin from *Clostridium perfringens*. *Biochemistry (Mosc.)* **46**, 11352-11360 (2007).
- 925 26. Boraston, A. B., Bolam, D. N., Gilbert, H. J. & Davies, G. J. Carbohydrate-binding
926 modules: fine-tuning polysaccharide recognition. *Biochem. J.* **382**, 769-781 (2004).
- 927 27. Singh, A. K. *et al.* Unravelling the multiple functions of the architecturally intricate
928 *Streptococcus pneumoniae* β -galactosidase, BgaA. *PLoS Pathog.* **10**, e1004364 (2014).
- 929 28. Qin, J. *et al.* A human gut microbial gene catalog established by metagenomic
930 sequencing. *Nature* **464**, 59-65 (2010).
- 931 29. Crost, E. H., Tailford, L. E., Le Gall, G., Fons, M., Henrissat, B. & Juge, N. Utilisation of
932 mucin glycans by the human gut symbiont *Ruminococcus gnavus* is strain-dependent. *PLoS*
933 *One* **8**, e76341 (2013).
- 934 30. Tailford, L. E. *et al.* Discovery of intramolecular *trans*-sialidases in human gut microbiota
935 suggests novel mechanisms of mucosal adaptation. *Nat. Commun.* **6**, 7624 (2015).
- 936 31. Crost, E. H. *et al.* The mucin-degradation strategy of *Ruminococcus gnavus*: The
937 importance of intramolecular *trans*-sialidases. *Gut Microbes* **25**, 1-11 (2016).
- 938 32. Ribeiro, J. P. *et al.* Characterization of a high-affinity sialic acid-specific CBM40 from
939 *Clostridium perfringens* and engineering of a divalent form. *Biochem J.* **473**, 2109-2118
940 (2016).
- 941 33. Luo, Y., Li, S. C., Chou, M. Y., Li, Y. T. & Luo, M., 1998. The crystal structure of an
942 intramolecular *trans*-sialidase with a NeuAc α 2 \rightarrow 3Gal specificity. *Struct. Lond. Engl.* **6**,
943 521-530 (1993).
- 944 34. Connaris, H., Crocker, P. R. & Taylor, G. L. Enhancing the receptor affinity of the sialic
945 acid-binding domain of *Vibrio cholerae* sialidase through multivalency. *J. Biol. Chem.* **284**,
946 7339-7351 (2009).
- 947 35. Yang, L., Connaris, H., Potter, J. A., Taylor, G. L. Structural characterization of the
948 carbohydrate-binding module of NanA sialidase, a pneumococcal virulence factor. *BMC*
949 *Struct. Biol.* **15**, 15 (2015).

- 950 36. Xu, G., Potter, J. A., Russell, R. J., Oggioni, M. R., Andrew, P. W. & Taylor, G. L. Crystal
951 structure of the NanB sialidase from *Streptococcus pneumoniae*. *J. Mol. Biol.* **1384**, 436-449
952 (2008).
- 953 37. Owen, C. D., Lukacik, P., Potter, J. A., Sleator, O., Taylor, G. L. & Walsh, M. A.
954 *Streptococcus pneumoniae* NanC: Structural insights into the specificity and mechanism of a
955 sialidase that produces a sialidase inhibitor. *J. Biol. Chem.* **290**, 27736-27748 (2015).
- 956 38. Padler-Karavani, V. *et al.* Cross-comparison of protein recognition of sialic acid diversity
957 on two novel sialoglycan microarrays. *J. Biol. Chem.* **287**, 22593-22608 (2012).
- 958 39. Deng, L., Chen, X. & Varki, A. Exploration of sialic acid diversity and biology using
959 sialoglycan microarrays. *Biopolymers* **99**, 650-665 (2013).
- 960 40. Mayer, M. & Meyer, B. Characterization of ligand binding by saturation transfer
961 difference NMR spectroscopy. *Ang. Chem. Int. Ed.* **38**, 1784-1788 (1999).
- 962 41. Angulo, J. & Nieto, P. M. STD NMR: application to transient interactions between
963 biomolecules-a quantitative approach. *Eur. Biophys. J.* **40**, 1357-1369 (2011).
- 964 42. Mayer, M. & Meyer, B. Group epitope mapping by saturation transfer difference NMR to
965 identify segments of a ligand in direct contact with a protein receptor. *J. Am. Chem. Soc.*
966 **123**, 6108-6117 (2001).
- 967 43. Marchetti, R., *et al.* Rules of engagement” of protein–glycoconjugate interactions: a
968 molecular view achievable by using NMR spectroscopy and molecular modeling. *Chemistry*
969 *Open* **5**, 274-296 (2016).
- 970 44. Thomsson, K. A., Holmén-Larsson, J. M., Angström, J., Johansson, M. E., Xia L. &
971 Hansson, G. C. Detailed O-glycomics of the Muc2 mucin from colon of wild-type, core 1- and
972 core 3-transferase-deficient mice highlights differences compared with human MUC2.
973 *Glycobiology* **22**, 1128-39 (2012).
- 974 45. Homquist, L. & Ostman, B. The anomeric configuration of N-acetylneuraminic acid
975 released by the action of *Vibrio cholerae* neuraminidase. *FEBS Lett.* **60**, 327-330 (1975).
- 976 46. Pell G., Williamson M. P., Walters C., Du H., Gilbert H. J. & Bolam D. N. Importance of
977 hydrophobic and polar residues in ligand binding in the family 15 carbohydrate-binding
978 module from *Cellvibrio japonicus* Xyn10C. *Biochemistry* **42**, 9316-9323 (2003).
- 979 47. Abbott, D. W. & van Bueren, A. L. Using structure to inform carbohydrate binding module
980 function. *Curr. Opin. Struct. Biol.* **28**, 32-40 (2014).
- 981 48. Etzold, S. *et al.* Structural basis for adaptation of lactobacilli to gastrointestinal mucus.
982 *Environ. Microbiol.* **16**, 888-903 (2014).
- 983 49. Gunning, A. P., Kavanaugh, D., Thursby, E., Etzold, S., MacKenzie, D. A. & Juge, N.
984 Use of atomic force microscopy to study the multi-modular interaction of bacterial adhesins
985 to mucins. *Int. J. Mol. Sci.* **17**, pii: E1854 (2016).
- 986 50. Varki, N. M., Strobert, E., Dick, E. J. J., Benirschke, K. & Varki, A. Biomedical differences
987 between human and nonhuman hominids: potential roles for uniquely human aspects of
988 sialic acid biology. *Annu. Rev. Pathol.* **6**, 365-393 (2011).
- 989 51. Tangvoranuntakul, P., *et al.* Human uptake and incorporation of an immunogenic
990 nonhuman dietary sialic acid. *Proc. Natl. Acad. Sci. U.S.A.* **100**, 12045-12050 (2003).
- 991 52. Ficko-Blean, E. & Boraston, A. B. Insights into the recognition of the human glycome by
992 microbial carbohydrate-binding modules. *Curr. Opin. Struct. Biol.* **22**, 570-577 (2012).
- 993 53. Hervé, C., Rogowski, A., Blake, A. W., Marcus, S. E., Gilbert, H. J. & Knox, J. P.
994 Carbohydrate-binding modules promote the enzymatic deconstruction of intact plant cell
995 walls by targeting and proximity effects. *Proc. Natl. Acad. Sci. U. S. A.* **107**, 15293–15298.
996 (2010).

- 997 54. El Kaoutari, A., Armougom, F. Gordon, J. I., Raoult, D. & Henrissat, B. The abundance
998 and variety of carbohydrate-active enzymes in the human gut microbiota. *Nat. Rev.*
999 *Microbiol.* **11**, 497-504 (2013).
- 1000 55. Yu, H. *et al.* Sequential one-pot multienzyme chemoenzymatic synthesis of
1001 glycosphingolipid glycans. *J. Org. Chem.* **81**, 10809-10824 (2016).
- 1002 56. Liu, H. & Naismith, J. H. A simple and efficient expression and purification system using
1003 two newly constructed vectors. *Protein Expr. Purif.* **63**, 102-111 (2009).
- 1004 57. Bergfors, T. Seeds to crystals. *J. Struct. Biol.* **142**, 66-76 (2003).
- 1005 58. Otwinowski, Z. & Minor, W. Processing of X-ray diffraction data collected in oscillation
1006 mode, in: *Macromolecular crystallography, Part A, Methods in enzymology.* Academic Press,
1007 New York, pp. 307–326 (1997).
- 1008 59. McCoy, A.J., Grosse-Kunstleve, R.W., Adams, P.D., Winn, M.D., Storoni, L.C. & Read,
1009 R.J. Phaser crystallographic software. *J. Appl. Crystallogr.* **40**, 658-674 (2007).
- 1010 60. Winn, M. D. *et al.* Overview of the CCP 4 suite and current developments. *Acta*
1011 *Crystallogr. D Biol. Crystallogr.* **67**, 235–242 (2011).
- 1012 61. Murshudov, G. N. *et al.* REFMAC5 for the refinement of macromolecular crystal
1013 structures. *Acta Crystallogr. D Biol. Crystallogr.* **67**, 355-367 (2011).
- 1014 62. Emsley, P., Lohkamp, B., Scott, W. G. & Cowtan, K. Features and development of Coot.
1015 *Acta Crystallogr. D Biol. Crystallogr.* **66**, 486-501 (2010).
- 1016 63. Joosten, R. P., Joosten, K., Murshudov, G. N. & Perrakis, A. PDB_REDO: constructive
1017 validation, more than just looking for errors. *Acta Crystallogr. D Biol. Crystallogr.* **68**, 484-496
1018 (2012).
- 1019 64. Chen, V. B. *et al.* MolProbity: all-atom structure validation for macromolecular
1020 crystallography. *Acta Crystallogr. D Biol. Crystallogr.* **66**, 12-21 (2010).
- 1021 65. Karplus, P. A. & Diederichs, K. Linking Crystallographic Model and Data Quality. *Science*
1022 **336**, 1030-1033 (2012).
- 1023 66. Finn, R. D. *et al.* The Pfam protein families database: towards a more sustainable future.
1024 *Nucleic Acids Res.* **44**, D279-285 (2016).
- 1025 67. Felsenstein, J. PHYLIP - Phylogeny Inference Package (Version 3.2). *Cladistics* **5**, 164-
1026 166 (1989).
- 1027 68. Rice, P. Longden, I. & Bleasby, A. EMBOSS: The European Molecular Biology Open
1028 Software Suite. *Trends Genet.* **16**, 276-277 (2000).
- 1029 69. Liquori, G. E. *et al.* In situ characterization of O-linked glycans of Muc2 in mouse colon.
1030 *Acta Histochem.* **114**, 723-732 (2012).

1031
1032 **Acknowledgements:** The authors gratefully acknowledge the support of the Biotechnology
1033 and Biological Sciences Research Council (BBSRC), this research was funded by the
1034 BBSRC Institute Strategic Programme for The Gut Health and Food Safety (BB/J004529/1),
1035 the BB/F016778/1 grant, and by the US National Institutes of Health (NIH) of grant
1036 R01HD065122 (to XC) and R01GM32373 (to AV). SM and JA acknowledge a postgraduate
1037 studentship and financial support from the School of Pharmacy of the University of East
1038 Anglia. We acknowledge Kathryn Cross (QIB) for the TEM analysis. We would like to thank

1039 Carmen Pin for her help with statistical analyses and Emmanuelle Crost for *R. gnavus*
1040 anaerobic culture.

1041

1042 **Author Contributions:** NJ conceived the study and wrote the manuscript with contribution
1043 from all co-authors. CDO carried out sub-cloning, produced the proteins (*RgCBM40*,
1044 *RgGH33*, *RgNanH*) and solved CBM40 crystal structures under GLT's supervision. LET
1045 carried out the cloning, heterologous expression, mutagenesis and CD analysis of proteins
1046 (*RgCBM40*, *RgGH33*, *RgNanH*) and carried out binding assays (ITC and ELISA) and
1047 enzyme kinetics (HPAEC), TS and LV carried out the immuno- histo/cytochemistry
1048 experiments, ST purified the mucins from human cell lines and mouse models, KL
1049 characterized the glycosylation profile of mucins by MS, MH contributed to the production of
1050 *RgCBM40*, *RgNanH* and *RgGH33*, and to CD and ELISA experiments. RL contributed to the
1051 production of *RgCBM40*, and to the CD and ITC experiments, AB performed the western
1052 blot analysis and prepared cells for TEM. AB, KL, LET, LV, ST, and TS worked under NJ's
1053 supervision, MH and RL worked under LET's supervision. JW performed the bioinformatics
1054 analyses. SM carried out the STD NMR experiments under JA's supervision, ZK performed
1055 the glycan microarray screening under AV's supervision, HY synthesized some of the
1056 sialosides used in this study under XC's supervision.

1057

1058 **Conflict of interest:** The authors declare no conflict of interest.

1059

1060

1061

1062 **Figure Legends**

1063

1064 **Figure 1 Crystal structure of RgCBM40 in complex with 3'SL and 6'SL** (a) *RgCBM40* is
1065 shown in a cartoon representation with a rotation of 90° around the x axis. (b) The protein
1066 crystallised as a dimer with the ligand binding site at the dimer interface. The binding sites
1067 are shown occupied by 6'SL trisaccharides (Neu5Ac: cyan, galactose: blue, glucose:
1068 orange). (c) SEC-MALS performed with full length *RgNanH* (77 kDa). The SEC-MALS
1069 predicted molecular weight was 73 kDa, indicating that *RgNanH* is monomeric in solution.
1070 Bound 3'SL (d) and 6'SL (e) are shown with their corresponding Fo-Fc omit maps at 2 σ
1071 (light cyan), 3 σ (orange), and 5 σ (magenta). The omit maps are carved at 1.6 Å around the
1072 bound ligand. For 3'SL, the map is carved around a dummy glucose residue to indicate the
1073 presence of partial electron density. A close-up view of *RgCBM40* binding site is shown with
1074 (f) 3'SL and (g) 6'SL. The Neu5Ac residue is shown in cyan and the galactose residue as
1075 black lines, for clarity the glucose residue is not shown. Interacting *RgCBM40* residues are
1076 shown in green with black dashed lines indicating hydrogen bonding interactions. A semi-
1077 transparent surface indicates the hydrophobic surface.

1078

1079 **Figure 2. CBM40 structural alignment**

1080 Structure-based alignment (α -helices and β -strands respectively in red and yellow) of
1081 CBM40 domains of *RgCBM40* with *C. perfringens* *CpCBM40_NanJ* (PDB code 2V73) and
1082 *CpCBM40_NanI* (PDB code 5FRA), *M. decora* *MdCBM40_NanL* (PDB code 1SLI) and *S.*
1083 *pneumoniae* *SpCBM40_NanA* (PDB code 4C1W), *SpCBM40_NanB* (PDB code 2VW0) and
1084 *SpCBM40_NanC* (PDB code 4YZ5) and *VcCBM40_NanH* structure (PDB code 2W68).
1085 Amino acids identified as binding sites are highlighted in blue. *RgCBM40* residues Ile95,
1086 Asp110, Tyr116, Glu126, Arg128, Arg204 and Tyr210 are at positions 104, 119, 125, 135,
1087 137, 226 and 233 of the alignment. The alignment supplemented with other canonical and
1088 *Vibrio*-type CBM40 sequences, used to create the pHMM using HMMER3, is shown in

1089 **Supplementary Fig. 4.**

1090

1091 **Figure 3. Distance-based tree of canonical and Vibrio-type CBM40 sequences**

1092 Tree of 51 non-redundant sequences (80% identity level) calculated by neighbour-joining
1093 using evolutionary distances estimated by applying the PMB model of amino acid changes,
1094 including all sites and using a uniform rate of evolution. The representative sequences
1095 corresponding most closely (at least 97% identical) to the 7 bacterial structure-determined
1096 sequences are shown with symbols, coloured in accordance with **Supplementary Fig. 1:**
1097 "A", *SpCBM40_NanA*; "B", *SpCBM40_NanB* "C", *SpCBM40_NanC*; "I", *CpCBM40_NanI*;
1098 "J", *CpCBM40_NanJ*; "R", *RgCBM40*; "V", *VcCBM40_NanH*. Additionally, "L" denotes

1099 *MdCBM40_NanL* closest to the bacterial sequence of highest identity (70% identical to
1100 *RgCBM40*) as only bacterial sequences were searched.

1101

1102 **Figure 4. Sialoglycan microarray analysis of binding specificities of *RgCBM40* and**
1103 ***RgGH33 D282A*.** Binding of the recombinant proteins *RgCBM40* and *RgGH33 D282A* at 20
1104 and 200 $\mu\text{g mL}^{-1}$, respectively are presented (n=4, SD). Heat map was generated using the
1105 method as previously described^{38,39}. Binding was ranked as (glycan average RFU/ maximum
1106 glycan average RFU)*100. Red and white represent the maximum and minimum,
1107 respectively. R1 represents propyl-azide as the spacer.

1108

1109 **Figure 5. STD NMR analysis of *RgCBM40* binding to sialoglycans, (a)** Reference (top)
1110 and difference (bottom) spectra of 3'SL and 6'SL. The strongest signals from the Neu5Ac's
1111 protons are labelled in the difference spectra. **(b)** Binding epitope mapping from STD NMR
1112 of 3'SL and 6'SL. Legend indicates relative STD intensities normalised at H7: blue, 0–24%;
1113 yellow, 25–50%, red 51–100%; larger red dots indicate values over 100%. Sialic acid is the
1114 main recognition element. **(c)** Binding epitopes mapping from STD NMR of Neu5Gc α 2-3Lac
1115 and Neu5Gc α 2-6Lac. Legend as above. Sialic acid is the main recognition element. The
1116 strongest STD intensities from CH2 and the H3s, suggest a reorientation of the Neu5Gc ring
1117 in the binding pocket, in comparison to 3'SL and 6'SL.

1118

1119 **Figure 6. ITC isotherms of *RgCBM40* to sialoglycans. (a)** *RgCBM40* binding to 3'SL, **(b)**
1120 *RgCBM40* binding to 6'SL, **(c)** *RgCBM40* binding to 3'SLGc, **(d)** *RgCBM40* binding to
1121 Neu5Ac. The Kd is indicated in mM. *This value is an estimate as the Kd is too high to
1122 determine with the concentration of sugar used.

1123

1124 **Figure 7. ELISA of *RgCBM40* binding to purified mucins.**

1125 **(a)** *RgCBM40* binding to a range of purified mucins; mucin 2 (MUC2) and mixed mucins
1126 (mucins) from human cell line LS174T, purified pig gastric mucin (pPGM), and murine
1127 mucins from germ free (GF), wild type (WT), and *C3GnT^{-/-}* mice. **(b)** Correlation of
1128 *RgCBM40* binding with % sialylated structure for each mucin tested. *RgCBM40* was
1129 incubated with immobilised mucins and binding determined by ELISA. The % sialylated
1130 structures was determined by MS. **(c)** *RgCBM40* binding to LS174T MUC2 which has been
1131 treated chemically (TFA) or enzymatically with a sialidase from *Clostridium perfringens* (*Cp*),
1132 *Salmonella typhimurium* (*St*), *Akkermansia muciniphila* (*Am*) or *Ruminococcus gnavus* (*Rg*)
1133 **(d)** *RgCBM40* binding to LS174T MUC2 in competition with sugars. *RgCBM40* has been
1134 preincubated with the indicated sugars. In all cases, *RgCBM40* was incubated with
1135 immobilised mucins and visualised by an ELISA using anti-sialidase primary antibody and an

1136 anti-rabbit secondary antibody conjugated to horseradish peroxidase. The enzyme was
1137 incubated with TMB and the absorbance at 450 nm (A450) measured. The error bars show
1138 the standard error of the mean (SEM) of three replicates. P values are indicated; NS-not
1139 significant, *-p<0.05, **-p<0.005, ***-p<0.005.

1140

1141 **Figure 8. *RgCBM40* binding to mucus-producing cells and intestinal tissue sections.**

1142 (a) Immunostaining pattern for *RgCBM40* on LS174T cells correlated with mucin (MUC2)
1143 and lectin (SNA) staining, all shown in green. No staining was observed in *RgCBM40*-free
1144 sample (Blank). (b) Immunostaining pattern for *RgCBM40* on cryosections of mouse colon
1145 correlated with mucin (Muc2) and lectin (SNA) staining, all shown in green. No staining was
1146 observed in *RgCBM40*-free sample (Blank). Cell nuclei were counterstained with DAPI,
1147 shown in blue. (c) Sialidase pre-treatment of mouse colonic cryosections markedly reduced
1148 the binding of *RgCBM40* and SNA lectin. Cell nuclei were counterstained with DAPI, shown
1149 in blue. (d) *RgCBM40* competition assay with SNA on cryosections of mouse colon.
1150 *RgCBM40* is shown in green. Cell nuclei were counterstained with DAPI, shown in blue. No
1151 *RgCBM40* specific staining was detectable when SNA was present. (e) *R. gnavus* binding
1152 competition assay with SNA on cryosections of mouse colon. *R. gnavus* ATCC 29149 was
1153 incubated on sequential cryosections of mouse colon with or without SNA treatment and is
1154 shown in red. The mucus layer is shown in green. Sequential sections were required as both
1155 antibodies were raised in the same species. Cell nuclei were counterstained with DAPI,
1156 shown in blue. No *R. gnavus* staining was detectable when SNA was present. Appropriate
1157 primary antibody and secondary antibody only controls are also shown underneath each
1158 panel, showing some background staining. Scale bar: 20 μ m.

1159

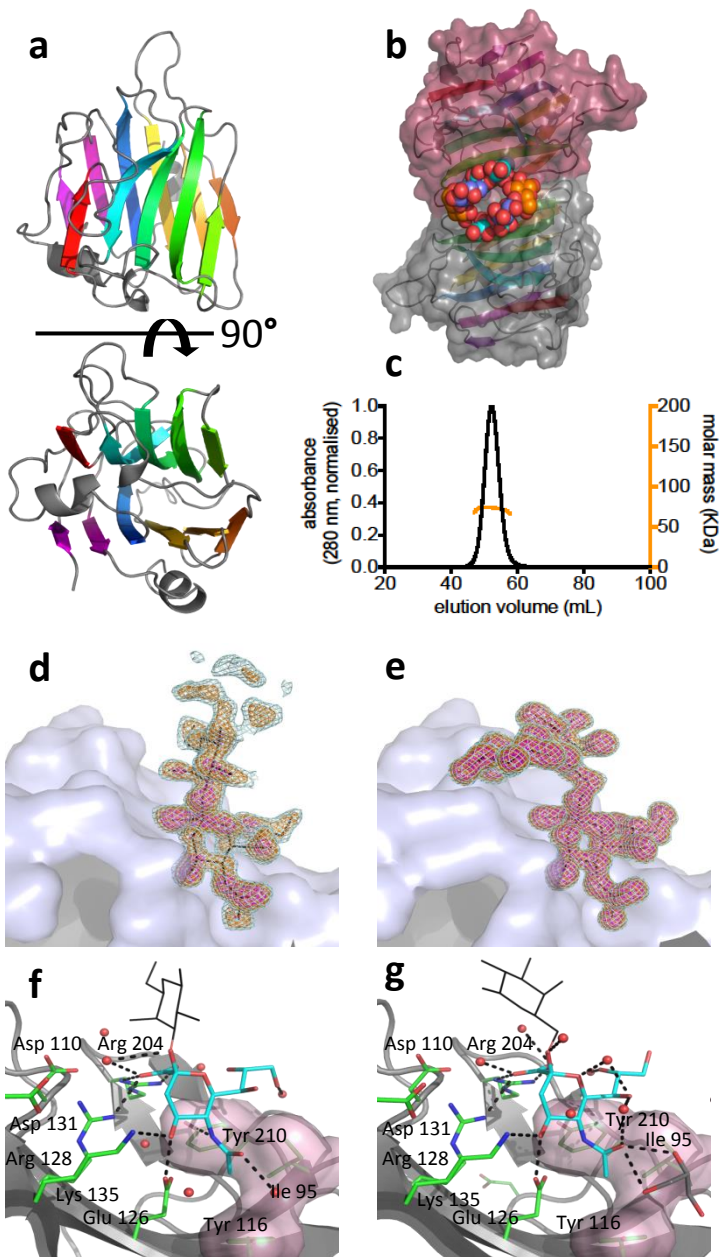
1160

1161

1162 **Table 1.** Data collection and refinement statistics. Values in parentheses refer to the highest
 1163 resolution shell. For the 3'SL and 6'SL complexes the data was over 90% complete to a
 1164 resolution of 1.85 Å and 1.56 Å respectively.
 1165

Dataset	Apo	3'SL	6'SL
Data collection			
Spacegroup	P21	P21	P21
Cell dimensions			
a, b, c (Å)	46.7, 72.8, 51.3	48.8, 72.4, 51.5	48.7, 72.2, 51.4,
β (°)	104.9	105.1	103.9
Resolution	50 – 1.73 (1.76 – 1.73)	39.48 – 1.37 (1.41 – 1.37)	49.91 – 1.30 (1.34 – 1.30)
R_{merge}	0.03 (0.14)	0.04 (0.34)	0.03 (0.15)
$I / \sigma I$	47.3 (9.6)	22.9 (3.0)	32.0 (4.9)
Completeness	91.8 (51.3)	74.5 (11.2)	83.9 (13.6)
Redundancy	3.7 (2.4)	4.3 (2.4)	5.1 (1.4)
Refinement			
Resolution	50 – 1.73 (1.76 – 1.73)	39.48 – 1.37 (1.41 – 1.37)	49.91 – 1.30 (1.34 – 1.30)
No. reflections	31570	51221	67097
$R_{\text{work}} / R_{\text{free}}$	0.160/0.194 (0.82)	0.152/0.187 (0.81)	0.134/0.154 (0.87)
No. of atoms	3145	3424	3704
Protein	2807	2850	3076
Ligand	0	81	123
Water	338	508	527
B-factors			
Protein	19.4	16.6	10.4
Ligand/ion		36.4	21.7
Water	28.1	31.7	27.3
R.m.s.d			
Bond lengths (Å)	0.011	0.012	0.015
Bond angle (°)	1.55	1.66	1.77

1166 *Values in parentheses are for the highest-resolution shell. One crystal was used for each
 1167 structure.
 1168
 1169
 1172



```

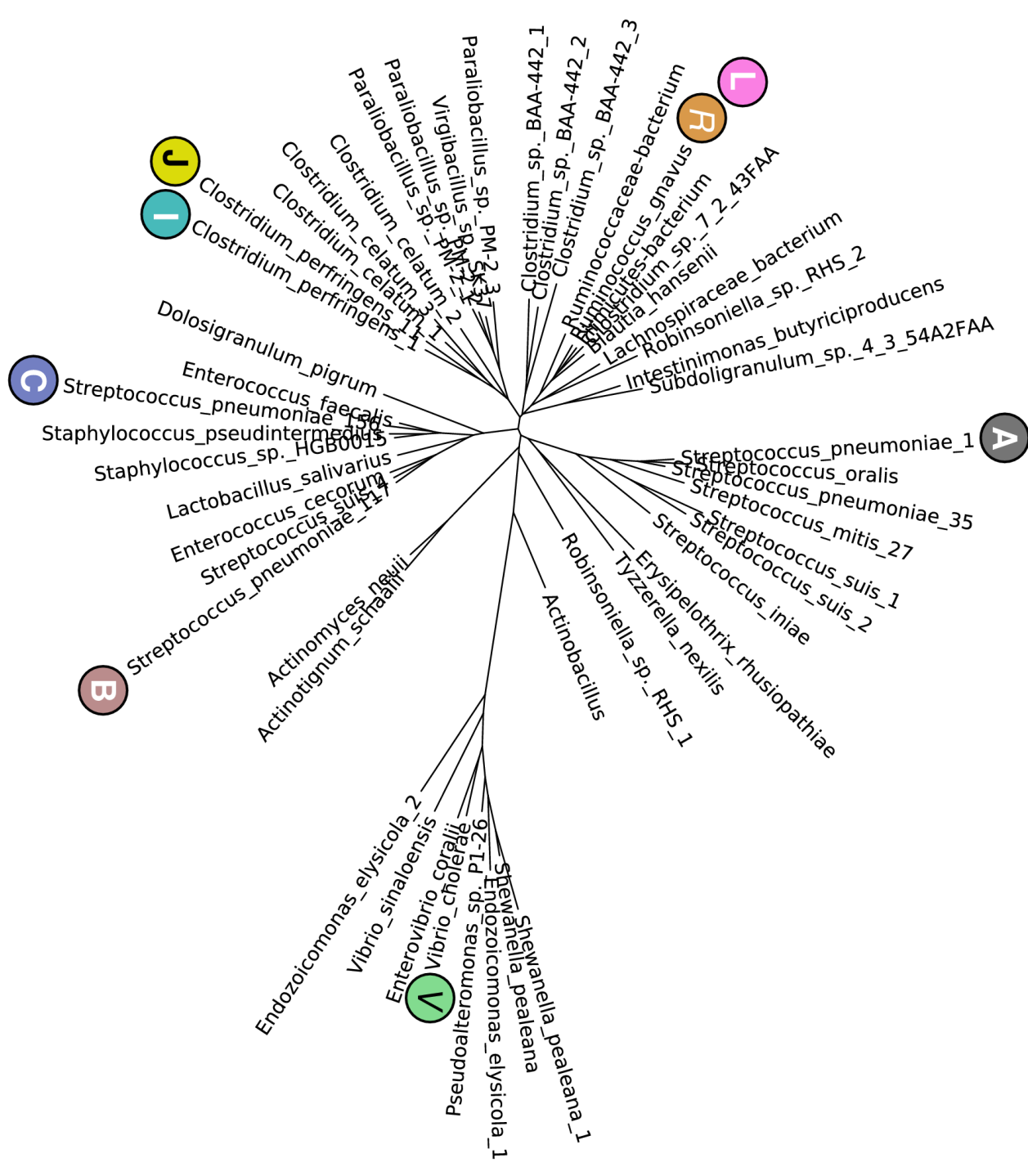
      10      20      30      40      50      60      70
SpCBM40_NanA -----VE--TVIEKEDVET-NASNGQ-----RVDL--SS-EL
SpCBM40_NanB -----IIFGGGSYQLN-N-K-S-----IDI--SLLL
SpCBM40_NanC -----PVLKKNVTLTG-G-G-----ENV--TKELK
CpCBM40_NanI ---SPDPNWELLSLGEYKDINL-ESSNA-----SNI--TY-DL
CpCBM40_NanJ LNVYEIKGEVD--EIIANYGNLKITKEEER-----VNI--TG-DL
McCBM40_NanL -----PEG--LLMEKNIVDI-AEGQG-----YSLDQEA-GA
RgCBM40 -----SV--PVLQKEGIEI-SEGTE-----YDLSKEP-GA
VcCBM40_NanH -----S-NAALFDYNI---ATGDTFEFDSPAKQGWMDNTNNGSGVLTNADGMPAWLVQGI GGRAGQWTYSL--STNQH

      90      100     110     120     130     140     150
SpCBM40_NanA DKLKKLENATVHMEFKPDAKAPAFYNLFSVSSATK--KDEYFTMAVYNN-TATLEPRGSG--DGKQ---FYN-NYNDAPLK
SpCBM40_NanB DKL-SGESQTVVMKFKADKP-NSLQALFGLSNKAGFKNNYFSIFMRDSGEIGVEIRD---AQK---GTN-YLFSRPAS
SpCBM40_NanC DKFTSGD-FTVVIKYNQSSSE-KGLQALFGISNSKPGQQMSYVDVFLRDNGELGMEARD--TSSN---KN-NLFSRPAS
CpCBM40_NanI EKYKNLDEGTIVVRFNS-KD-SKIQLLGLISNSK--TKNGYFNRYVTNS-RVGFELRNQKNEGNTQGTENLVHMYKQVA
CpCBM40_NanJ EKFSSELEGTIVTRFNM-ND-TSIIQSLIGLSDGNK--ANNYFSLYVS-GGKVGYEELRR--QEGNG--DEN-VHHSADVT
McCBM40_NanL KYVKAMTQGTIILSYKSTSE-NGIQSLFSVGNSTAGNQDRHFHLYITNSGGIGIELRN--TDGV----FN-YTLDRPAS
RgCBM40 ATVKALEQGTIVISYKTTSE-NAIQSLLSVGNSTAGNQDRHFHLYITNAGGVGMEELRN--TDGE----FK-YTLDCPAA
VcCBM40_NanH AQASS-FGWRMTTEMKVLSSG---GMITNYIYANG--TGRVLPILISLSSGNLVVER----EGQT---GR--TVLATGT

      170     180     190     200     210     220     230
SpCBM40_NanA VKP---GQW--NSVTFITVEKPTAELPKGRVRLYVNGVLSRT-SLRSGNFIDKMPDVTHVQIGA TKRAN-NTVW-GSNLQI
SpCBM40_NanB LWGKHKGQAVENTLVFVSDSKDK-----TYTMYVNGIEVFSETVDTFLPISN INGIDKATLGA VNRRE-GKEHY-LAKGSI
SpCBM40_NanC VWGKYKQEAVENTVAVVADSVKK-----TYSLYANGTKVVEKVDNFLN IKD IKGIDYMLGGVKRA-GKTA F-GFNGTL
CpCBM40_NanI L---NDGD--NTVALKIEKN-----KGYKFLNGKMIKEVDNTNTKFLNNIENLDSAFIGKTNRYGQSNEY-NFKGNI
CpCBM40_NanJ F---NRGI--NTLALKIEK-----GIAKIFLNGSLVKTVDPNIKFLNAIENLNSGFIGKTRANGYNEY-LFRGNI
McCBM40_NanL VRALYKGERVFNVALKADAANK-----QCRLFANGELLATLDKDAFKFISDITGVNDVTLGGTKRQ-GKIAY-PFGGTI
RgCBM40 VRGSYKGERVSNVALKADKENK-----QYKLFANGELIATLDQEAFFISDITGVNDVMLGGTMRQ-GTVAY-PFGGSI
VcCBM40_NanH AATEY-----HKFELVFPGSNP-----SASFYFDGKLIRDNIOPTA-----SKQNMIVWGN-----GSSNTDGVAAAY

      250     260
SpCBM40_NanA RNLTVYNRALTPEEVQKRSQLFK
SpCBM40_NanB DEISLFNKALSDQEVSTIPLSNP
SpCBM40_NanC ENIKFNSALDEETVKKMTINA-
CpCBM40_NanI GFMNIYNEPLGDDYLLSKTGETK
CpCBM40_NanJ DFMNIYDKPVSQNYLLRKTGETK
McCBM40_NanL GDIKVSNALSDDEELIQATGVTT
RgCBM40 ERMQVYRDVLSDDDELIAVTGKT-
VcCBM40_NanH RDIKFEIQGD-----

```



Glycan Structure	RgCBM40	RgGH33 D282A	Rank
Neu5Ac6GalNAc6R1			100
Neu5Ac6GalB4GlcNAc6R1			50
Neu5Ac6GalB3GlcNAc6R1			0
Neu5Ac6GalB3GalNAc6R1			
Neu5Ac6GalB4GlcNAc6R1			
Neu5Ac6GalB4Glc6R1			
Neu5Ac6GalB4Glc6R1			
Neu5Ac6GalB6R1			
Neu5Ac6GalB6R1			
Neu5Ac6GalB3GalNAc6R1			
Neu5Ac6Neu5Ac6GalB4Glc6R1			
Neu5Ac6Neu5Ac6Neu5Ac6GalB4Glc6R1			
Neu5Ac6GalB4(Fuco3)GlcNAc6R1			
Neu5Ac6GalB4(Fuco3)GlcNAc6S6R1			
Neu5Ac6GalB3GlcNAc6B3GalB4Glc6R1			
Neu5Ac6GalB4GlcNAc6S6R1			
Neu5Ac6(Neu5Ac6)GalB4Glc6R1			
Neu5Ac6(Neu5Gco3)GalB4Glc6R1			
Neu5Ac6(Kdnc3)GalB4Glc6R1			
Neu5Ac6Neu5Gco3GalB4Glc6R1			
Neu5Ac6Neu5Gco6GalB4Glc6R1			
Neu5Ac6Neu5Ac6GalB4Glc6R1			
Neu5Ac6GalB4GlcNAc6R1			
Neu5Ac6GalB4GlcNAc6R1			
Neu5Ac6GalB3GlcNAc6R1			
Neu5Ac6GalB3GalNAc6R1			
Neu5Ac6GalNAc6R1			
Neu5Ac6GalB6R1			
Neu5Ac6GalB6R1			
Neu5Ac6GalB3GalNAc6R1			
Neu5Ac6GalB4Glc6R1			
Neu5Ac6GalB4Glc6R1			
Neu5Gco6GalNAc6R1			
Neu5Gco3GalB4GlcNAc6R1			
Neu5Gco3GalB3GlcNAc6R1			
Neu5Gco3GalB3GalNAc6R1			
Neu5Gco6GalB4GlcNAc6R1			
Neu5Gco6GalB4Glc6R1			
Neu5Gco3GalB4Glc6R1			
Neu5Gco3GalB6R1			
Neu5Gco6GalB6R1			
Neu5Gco3GalB3GalNAc6R1			
Neu5Gco3GalB4(Fuco3)GlcNAc6R1			
Neu5Gco3GalB4(Fuco3)GlcNAc6S6R1			
Neu5Gco3GalB3GlcNAc6B3GalB4Glc6R1			
Neu5Gco3GalB4GlcNAc6S6R1			
Neu5Gco8Neu5Ac6GalB4Glc6R1			
Neu5Gco8Neu5Gco3GalB4Glc6R1			
Neu5Gc9Ac6GalB4GlcNAc6R1			
Neu5Gc9Ac6GalB4GlcNAc6R1			
Neu5Gc9Ac6GalB3GlcNAc6R1			
Neu5Gc9Ac6GalB3GalNAc6R1			
Neu5Gc9Ac6GalNAc6R1			
Neu5Gc9Ac6GalB6R1			
Neu5Gc9Ac6GalB6R1			
Neu5Gc9Ac6GalB3GalNAc6R1			
Neu5Gc9Ac6GalB4Glc6R1			
Neu5Gc9Ac6GalB4Glc6R1			
Kdnc8Neu5Ac6GalB4Glc6R1			
Kdnc8Neu5Gco3GalB4Glc6R1			

